Distinct Developmental Functions for Cytoplasmic Actin Isoforms

A DISSERTATION
SUBMITTED TO THE FACULTY OF THE GRADUATE SCHOOL
OF THE UNIVERSITY OF MINNESOTA
BY

Tina M. Bunnell

IN PARTIAL FULFILLMENT OF THE REQUIREMENTS
FOR THE DEGREE OF
DOCTOR OF PHILOSOPHY

James M. Ervasti, Advisor

DECEMBER 2010

Acknowledgements

I owe a special thank you to Jim for being such a supportive and influential mentor. Jim encourages independent thinking and allowed me the freedom to develop my own ideas, yet when needed he was always available for helpful guidance. Jim's mentorship has been instrumental to my development as a scientist.

I would also like to thank both past and present Ervasti lab members for making the lab such an enjoyable place to work. I owe a special acknowledgement to KJS who initiated the development of our β_{cyto}- and γ_{cyto}-actin knockout mouse models. Additionally, I would like to thank my fellow comrades in actin isoform research, Ben and Tom, for all the valuable advice over the years.

I am incredibly grateful to my loving and supportive family, whose hard work and success have been an inspiration. And last but not least, I would like to thank my husband Jon, who has been more than supportive throughout the years and is an all around truly amazing husband.

Abstract

Actins are among the most highly expressed proteins in eukaryotes and play a critical role in most cellular processes. In mammals there exists six different actin isoforms, of which only the cytoplasmic β_{cyto}- and γ_{cyto}-actins are ubiquitously expressed. Remarkably, the cytoplasmic actins differ at only 4 out of 375 amino acids and have been exactly conserved from birds to mammals. It has been postulated that β_{cyto}- and γ_{cyto}-actin have distinct biological functions; therefore, to test this hypothesis we generated null alleles of the *Actb* and *Actg1* genes. Characterization of the resulting isoform-specific null animals demonstrates that β_{cyto}-actin but not γ_{cyto}-actin is essential for embryonic viability. While γ_{cyto}-actin is largely dispensable for embryonic development, it does confer growth and survival advantages, as evidenced by the fact that γ_{cyto}-actin null embryos exhibited mild developmental delays and decreased postnatal survival. Furthermore, γ_{cyto}-actin null primary mouse embryonic fibroblasts (MEFs) had a mild growth deficiency and a slight increase in apoptosis, despite total actin levels being maintained. In contrast to γ_{cyto}-actin null mice, β_{cyto}-actin null mice were early embryonic lethal, indicating that β_{cyto}-actin is an essential gene required for embryogenesis. The lethality in β_{cyto}-actin null mice is likely due to defects in cell growth and migration as these processes were severely impaired in β_{cyto}-actin knockout primary MEFs. Together, the distinct phenotypes observed in β_{cyto}- and γ_{cyto}-actin knockout mice and cells demonstrate that while β_{cyto}- and γ_{cyto}-actin can compensate for each other to a limited extent, they also have unique biological functions.

Table of Contents

List of Tables

Chapter 1

Chapter 2

Chapter 3

Appendix

List of Figures

Chapter 1

Chapter 2

Chapter 3

Appendix

List of Abbreviations

α_{ca}-actin	α-cardiac muscle actin
α_{sk}-actin	α-skeletal muscle actin
α_{sm}-actin	α-smooth muscle actin
β_{cyto}-actin	β-cytoplasmic actin
γ_{cyto}-actin	γ-cytoplasmic actin
γ_{sm}-actin	γ-smooth muscle actin
ABPs	Actin binding proteins
ADF	Actin-depolymerizing factor
ADP	Adenosine disphosphate
ANOVA	Analysis of variance
Ao	Aorta
Arp2/3	Actin-related protein 2/3 complex
Ate1	Arginyltransferase 1
ATP	Adenosine triphosphate
CD4	Cluster of differentiation 4
CPT	Camptothecin
DNA	Deoxyribonucleic acid
E	Embryonic day
F-actin	Filamentous actin
FITC	Fluorescein isothiocyanate

G-actin	Globular actin
kDa	Kilodalton
LV	Left ventricle
MEFs	Mouse embryonic fibroblasts
mRNA	Messenger RNA
MRTFs	Myocardin-related transcription factors
N-terminus	Amino-terminus
PCR	Polymerase chain reaction
PI	Propidium Iodide
RNA	Ribonucleic acid
RV	Right ventricle
Scar	Suppressor of cyclic AMP receptor
siRNA	Small interfering RNA
SRF	Serum response factor
UTR	Untranslated region
VS	Ventricular septum
WASp	Wiskott-Aldrich syndrome protein
ZBP1	Zipcode binding protein 1

Chapter 1

Introduction

Actin Dynamics and Regulation

Actin is a 42 kDa protein that is highly expressed in all eukaryotic cells and plays a fundamental role in most cellular processes through its ability to reversibly polymerize into stiff filaments. Actin filaments are double helical polymers with molecular polarity owing to the fact that the asymmetric globular subunits all have the same orientation. One end of the filament is known as the barbed end and the other as the pointed end. The polarity of filaments is important as the two ends have different rate constants and different affinities for proteins that regulate actin dynamics.

In the monomeric state, actin binds ATP in a deep cleft between its two lobes. Soon after assembly into filaments, actin hydrolyzes the ATP to ADP and dissociates the γ-phosphate (Figure 1.1). While ATP stabilizes monomeric actin, it is not required for polymerization (1). Rather, ATP hydrolysis and phosphate dissociation appear to provide an internal timer for the age of the filament and regulates filament disassembly through interactions with regulatory proteins.

Under physiological conditions *in vitro*, actin monomers spontaneously polymerize into filaments (2). Initiation of a filament is called nucleation, as actin monomers must first form a small oligomer called a nucleus. These small oligomers are very unstable, making nucleation the rate-limiting step in actin polymerization. Once a nucleus is formed filaments grow rapidly by the addition of monomers to both ends, however, the rate of elongation is greater at barbed ends than pointed ends. Actin polymerization is reversible as filaments can also depolymerize by the dissociation of actin subunits. Thus, a dynamic equilibrium between actin monomers and filaments

exists and is dependent on the concentration of free monomers. The dissociation equilibrium constant for monomer binding at the end of a polymer is called the critical concentration and differs at each end of the filament (Figure 1.1). Polymerization occurs when monomeric actin is above the critical concentration and depolymerization favored when monomeric actin is below the critical concentration. Therefore, once a steady-state is reached the concentration of monomers is slightly above the critical concentration at the barbed end and below that at the pointed end, resulting in a net addition of subunits at the barbed end and net loss at the pointed end. This slow flux of subunits through the filament is known as treadmilling and occurs when the monomer concentration is intermediate between the critical concentrations for the barbed and pointed ends.

The spontaneous self-assembly and treadmilling of actin filaments observed *in vitro* cannot alone account for the many physiological roles of actin; therefore, eukaryotic cells have more than 100 actin binding proteins (ABPs) that function to regulate actin. A large number of ABPs regulate the assembly and disassembly of actin filaments (3). Given that spontaneous nucleation is highly unfavorable, cells use proteins such as the Arp2/3 complex and formins to initiate new filaments. Arp2/3 is a well-studied protein complex that can nucleate filaments from the side of existing filaments and plays an important role in expanding the network of filaments at the leading edge of motile cells. Additionally, many ABPs serve to regulate filament growth and disassembly. For example, capping proteins can control filament length. Capping proteins that bind the barbed end of filaments inhibit filament growth, while those that bind the pointed end reduce the loss of monomers from the filament, thereby promoting filament extension.

Other proteins function to drive filament disassembly, such as the actin-depolymerizing factor (ADF) and the cofilin family of proteins. Some ABPs can also sever actin filaments, which rapidly increases actin dynamics. Severing proteins mostly function to disassemble filaments but they can also function to provide new barbed ends for filament growth. Finally, a set of monomer binding proteins allows for the availability of actin monomers to be tightly regulated. Many cellular functions, such as migration, require rapid filament growth; therefore, a large pool of monomers, poised for polymerization, must be maintained in the cell. This is achieved through monomer-sequestering proteins, such as the thymosin family, which bind actin and prevent polymerization. Appropriate signals then trigger the release of thymosin binding, resulting in a massive increase in the amount of monomeric actin available for polymerization. Profilin, another actin monomer binding protein, facilitates the exchange of ADP for ATP and prevents nucleation and elongation of pointed ends but not barbed ends.

Another important set of actin binding proteins serves to organize actin into networks and higher-order structures that are essential to a cell's form and function (4). Actin-bundling proteins, such as fimbrin and α-actinin, bundle actin filaments into linear arrays that are either loosely or tightly bundled depending on the architecture of the bundling protein. In contrast, actin crosslinking proteins, such as filamin and spectrin, organize filaments into orthogonal arrays, the nature of which depends on the ABP.

Lastly, a group of ABPs utilize actin filaments as a scaffold, physical support or track (5). Some of these proteins function to connect actin to membranes or other cytoskeletal networks, thereby providing a structural framework within cells. In contrast,

the large superfamily of molecular motor proteins known as myosins utilizes the actin cytoskeleton to produce mechanical force and movement. In an ATP-dependent manner, myosin generates force between actin filaments to produce the contractions necessary for a variety of cellular processes. In addition, myosin can move organelles and macromolecular complexes along actin filaments over short distances.

Figure 1.1: Actin treadmilling *in vitro*. Rate constants for the association ($\mu M^{-1}s^{-1}$) and dissociation (s^{-1}) of ATP-actin and ADP-actin at both ends of the actin filament are shown. The ratio of the dissociation rate constant to the association rate constant gives the dissociation equilibrium constant K (μM), also known as the critical concentration. The critical concentrations for ATP-actin differ at the two ends, giving rise to a slow steady state treadmilling. After assembly into filaments, ATP is rapidly hydrolyzed, followed by dissociation of the phosphate. T signifies ATP-bound actin and D signifies ADP-bound actin. Adapted from (6).

Figure 1.1

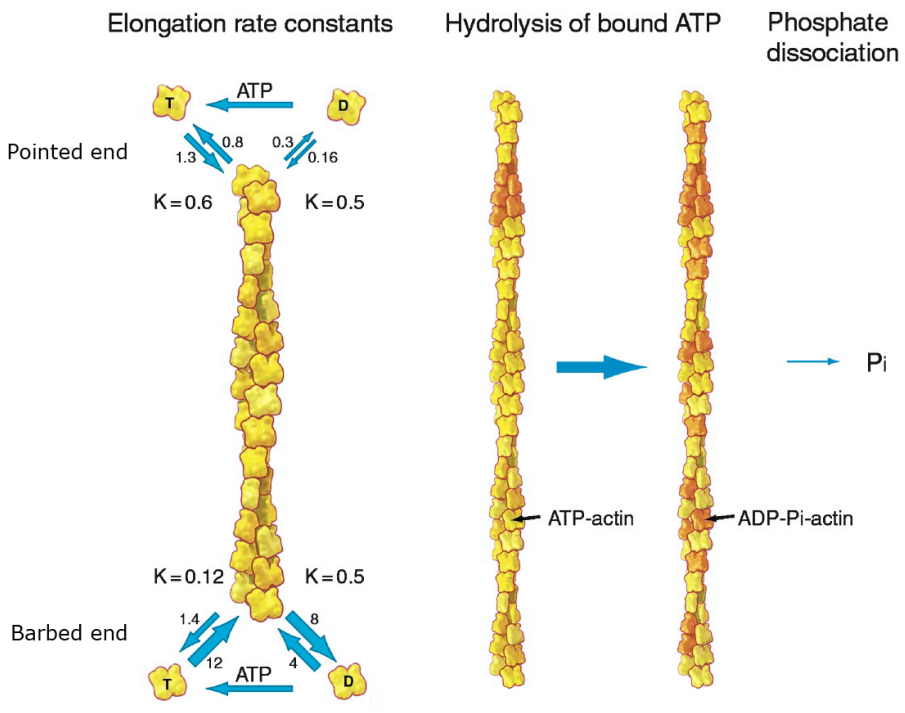
Elongation rate constants
Hydrolysis of bound ATP
Phosphate dissociation
ATP
T
D
Pointed end
1.3
0.8
0.3
0.16
K=0.6
K=0.5
K=0.12
K=0.5
Barbed end
1.4
12
8
4
ATP
T
D
ATP-actin
ADP-Pi-actin
Pi

Cellular Functions of Actin

Actin was first identified in muscle where it provides a scaffold on which myosin can generate force for muscle contraction. It is now known that actin plays an important role in nearly all cell types and cell behaviors (7). As a component of the cytoskeleton, actin provides the mechanical support required for the establishment and maintenance of cell shape and polarity. Actin filaments can be organized into a variety of different arrangements that form a diverse array of cellular structures, such as microvilli, stress fibers and lamellipodia, which are critical to the cell's function. Actin filaments also play a role in internalization of membrane vesicles as well as provide tracks for cargo transport by myosin. Additionally, actin dynamics feed into the serum response factor (SRF) gene regulatory pathway such that the level of monomeric actin in a cell regulates the expression of SRF target genes (8). Many of these target genes include actin and actin regulators, thus it appears that actin itself is part of an autoregulatory feedback circuit that links actin dynamics with transcriptional regulation. Furthermore, actin has been shown to associate with chromatin remodeling complexes and all three RNA polymerases, implicating a direct role for actin in gene transcription (9).

Actin also plays a critical role in cytokinesis, a complicated process involving more than 100 proteins (10). During late stages of cell division a contractile ring, composed of myosin and actin filaments, assembles equatorially at the cell cortex (Figure 1.2A). The thin band of actin filaments is attached to the plasma membrane such that as myosin pulls filaments together the cell membrane ingresses. As the contractile ring constricts, actin filaments depolymerize in proportion to the circumference.

One of the most well studied roles for actin is in cell motility, a fundamental process essential for embryonic development, wound healing, and immune responses. During cell migration four coordinated events occur: initial extension of a membrane protrusion, adhesion to the substratum, forward flow of cytosol, and retraction of the rear of the cell. Cell protrusions, or lamellipodia, extend by polymerization of actin filaments, which provide the necessary force to push the membrane forward and drive cell locomotion (Figure 1.2B) (6). Lamellipodia contain a branched network of actin filaments with barbed ends oriented outward from the cell. Branching is achieved through activation of the Arp2/3 complex, which mediates the initiation of new filaments as branches on preexisting filaments. As actin filaments elongate by assembly of monomeric actin onto barbed ends, the leading edge membrane is pushed forward. Since short filaments are stiffer than long filaments and are therefore more effective at pushing on the membrane, filaments are typically capped before growing longer than 0.5 μm. A short distance behind the leading edge, actin filaments are disassembled with the help of ADF/cofilin proteins. Profilin subsequently catalyzes the exchange of ADP for ATP, thus replenishing the pool of actin monomers ready for elongation at the leading edge. In order to provide the adhesive traction for cell movement, actin bundles within lamellipodia form stable contacts, called focal adhesions, with the underlying substratum. As the contents of the cell are translocated forward through a myosin-dependent mechanism the focal adhesions eventually assume positions toward the back of the cell where they are disassembled.

Through its many cellular functions, the actin cytoskeleton plays an essential role in embryonic development. Most notably, the actin cytoskeleton provides the mechanical forces that drive embryonic morphogenesis, a process that controls the organized spatial distribution of cells and causes an organism to develop its shape. Two types of actin-based forces drive morphogenetic movements: protrusive and contractile (11). Actin polymerization provides the protrusive force that drives cells forward, allowing cells to migrate along predetermined paths. In contrast, actin filaments together with myosin motors generate the contractile forces that reorganize entire groups of cells into distinct embryonic structures. This type of collective cell movement results from the fact that actin filaments are anchored to the plasma membrane at sites of cell-cell adhesion, allowing the actin cytoskeleton of an entire tissue to act as a single mechanical structure.

In addition to providing the necessary forces for embryonic morphogenesis, the actin cytoskeleton is important for other aspects of development. For example, during embryogenesis cells must rapidly proliferate, requiring reorganization of the actin cytoskeleton and formation of an actin-myosin contractile ring. Furthermore, the actin cytoskeleton provides mechanical support to cells, dictates cell shape and helps establish polarity, and forms the basis of specialized cellular structures necessary for the cell's function.

Figure 1.2: Examples of actin-based cellular processes. A: During cytokinesis, a contractile ring composed of actin filaments and myosin assembles equatorially at the cell cortex. The contractile ring constricts as myosin pulls actin filaments together, causing the cell membrane to ingress. **B:** Actin polymerization at the leading edge drives membrane extension and cell locomotion. Upon receiving the appropriate extracellular signals, the Arp2/3 complex becomes activated by WASp/Scar proteins and initiates new filament growth as branches on preexisting filaments. Rapid growth at the barbed end of the new branch pushes the membrane forward. Capping proteins terminate filament elongation before the filaments become too long. Filaments age by hydrolysis of ATP (white subunits turn yellow) followed by dissociation of the phosphate (subunits turn red), thus marking the filament for disassembly by ADF/cofilin. Profilin subsequently binds actin monomers and catalyzes the exchange of ADP for ATP. A pool of ATP-actin bound to profilin is then ready to elongate barbed ends as they become available at the leading edge. Adapted from (7).

Figure 1.2

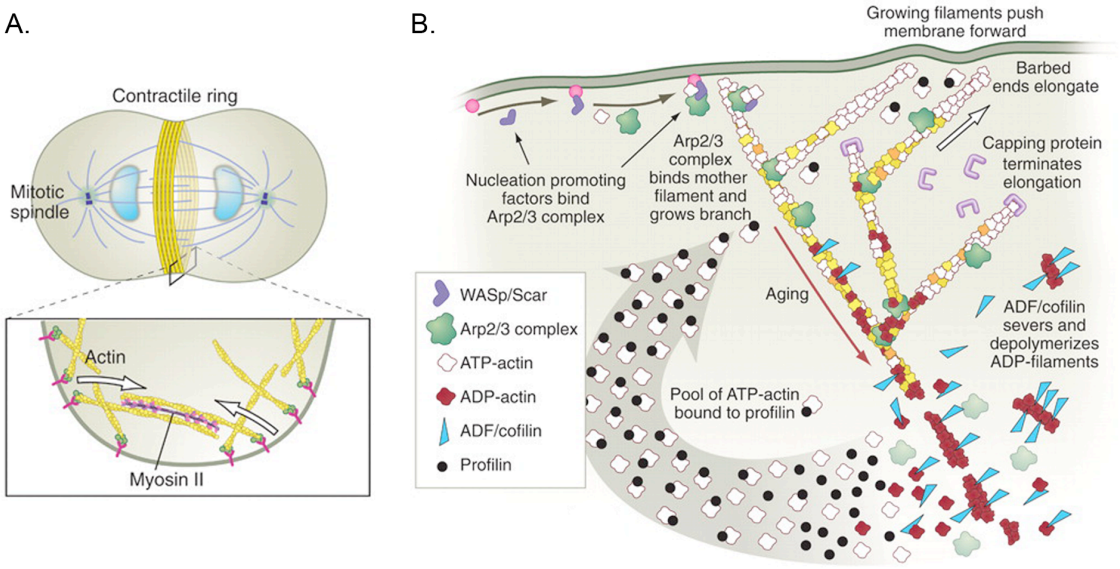
A.
Contractile ring
Mitotic spindle
Actin
Myosin II
B.
Growing filaments push membrane forward
Barbed ends elongate
Capping protein terminates elongation
Arp2/3 complex binds mother filament and grows branch
Nucleation promoting factors bind Arp2/3 complex
Aging
ADF/cofilin severs and depolymerizes ADP-filaments
Pool of ATP-actin bound to profilin
WASp/Scar
Arp2/3 complex
ATP-actin
ADP-actin
ADF/cofilin
Profilin

Mammalian Actin Isoforms

In mammals there exists six different actin isoforms expressed in a tissue specific pattern (12). Four of the actin isoforms are muscle specific: α_{smooth}-actin and γ_{smooth}-actin are predominately expressed in smooth muscle, while $\alpha_{cardiac}$-actin and $\alpha_{skeletal}$-actin are expressed in cardiac and skeletal muscle, respectively. The remaining two isoforms are termed cytoplasmic actins (β_{cyto}-actin and γ_{cyto}-actin) due to their ubiquitous expression in all cell types. Actin isoforms are each encoded by different genes, yet share a very high degree of protein sequence homology (13). The two most divergent isoforms differ by less than 7% of their primary sequence, while the cytoplasmic actins remarkably differ at only 4 out of 375 amino acids. These 4 divergent residues reside in the first 10 N-terminal amino acids and are biochemically very similar between the two isoforms (Table 1.1). Importantly, all six isoforms have been exactly conserved from birds to mammals, implicating functional specificity for each isoform.

Table 1.1: N-terminal sequences of mammalian actin isoforms

β_{cyto}-actin	Ac -D-D-D- I -A-A-L-V-V-D-N-G- S -G-M-C-K-
γ_{cyto}-actin	Ac -E-E-E- I -A-A-L-V- I -D-N-G- S -G-M-C-K-
γ_{smooth}-actin	Ac -E-E-E-T-T-A-L-V-C-D-N-G- S -G-L-C-K-
α_{smooth}-actin	Ac -E-E-E-D- S -T-A-L-V-C-D-N-G- S -G-L-C-K-
$\alpha_{cardiac}$-actin	Ac -D-D-E-E-T-T-A-L-V-C-D-N-G- S -G-L-V-K-
$\alpha_{skeletal}$-actin	Ac -D-E-D-E-T-T-A-L-V-C-D-N-G- S -G-L-V-K-

Ac- denotes an acetyl group. Red boxes indicate amino acid differences between cytoplasmic actin isoforms. Modified from (13).

Functional Specificity of Actin Isoforms

Functional specificity between muscle actins is evidenced by the fact that knockout of individual muscle-specific actin-isoforms in mice results in distinct phenotypes. Knockout of $\alpha_{cardiac}$-actin, α_{smooth}-actin, or $\alpha_{skeletal}$-actin resulted in defects in cardiac, smooth, or skeletal muscle respectively (14-16). Furthermore, transgenic overexpression of γ_{smooth}-actin was unable to fully rescue the defects in $\alpha_{cardiac}$-actin knockout mice and overexpression of γ_{cyto}-actin did not rescue the phenotypes of $\alpha_{skeletal}$-actin knockout mice (14, 17). Together, these data indicate distinct cellular functions for each muscle-specific actin isoform. While the cytoplasmic actin isoforms are 99% identical and ubiquitously expressed, several lines of evidence suggest that β_{cyto}- and γ_{cyto}-actin also have some functional specificity.

β_{cyto}-Actin and γ_{cyto}-actin are coexpressed in all cell types; however, their relative expression is under strict temporal and spatial regulation (18-21). Throughout embryonic development β_{cyto}- and γ_{cyto}-actin exhibit distinct patterns of expression in both space and time (20). By adulthood, cytoplasmic actins are expressed at a ratio of approximately 2:1 β_{cyto}- to γ_{cyto}-actin; however, exceptions exist in some tissues (18-21). Notably, β_{cyto}- and γ_{cyto}-actin can regulate the synthesis of one another as perturbations in the expression of one of the isoforms leads to concomitant changes in the expression of the other such that total actin levels are maintained (22, 23). Cytoplasmic actin expression is thus a highly regulated and complex process resulting in distinct spatial and temporal expression patterns between β_{cyto}- and γ_{cyto}-actin. These different expression patterns are thought to reflect different functional requirements for the two isoforms.

In addition to tissue-specific expression differences, β_{cyto}- and γ_{cyto}-actin mRNA and protein have been shown to differentially localize within cells. In cultured endothelial cells and 3T3 fibroblasts β_{cyto}-actin was strictly localized to the leading edge of motile cytoplasm after mechanical injury (24). The appearance of β_{cyto}-actin at the wound edge correlated with a two- to threefold increase in β_{cyto}-actin mRNA levels, which rose within 15-60 min after injury. In myoblasts, β_{cyto}-actin but not γ_{cyto}-actin mRNA was localized to the cell periphery, such as in extending processes and membrane ruffles, regions that reflect cell movement (25). Furthermore, in developing neurons β_{cyto}-actin was found to localize to growth cones and other actively growing structures, while γ_{cyto}-actin was uniformly distributed throughout the cell (26, 27). The observed enrichment of β_{cyto}-actin at the leading edge of migrating cells has led to the hypothesis that β_{cyto}-actin is the main actin isoform that drives protrusion formation.

Preferential targeting of β_{cyto}-actin to the leading edge is thought to occur in part by zipcode binding protein 1 (ZBP1)-mediated asymmetric localization and translation of β_{cyto}-actin mRNA. The 3'-untranslated region of β_{cyto}-actin mRNA contains a zipcode binding sequence not found in γ_{cyto}-actin mRNA that is recognized by ZBP1 (28, 29). Binding of ZBP1 in turn promotes transport of β_{cyto}-actin mRNA to the cell periphery while preventing translation initiation (30, 31). Once at the cell periphery, ZBP1 is released from the mRNA, thereby permitting localized translation (31). Interference with β_{cyto}-actin mRNA-ZBP1 binding using antisense oligonucleotides against the zipcode sequence resulted in reduced fibroblast motility (32) and blocked growth cone turning in response to guidance cues (33). These studies suggest that ZBP1-mediated asymmetric

transport and translation of β_{cyto}-actin mRNA is important for cell motility. It is worth noting that ZBP1 is known to associate with numerous mRNAs, including many other cytoskeletal-related proteins (34), suggesting that β_{cyto}-actin may be part of an integrated cellular program that coordinately regulates mRNAs encoding functionally related proteins.

The hypothesis that β_{cyto}-actin enrichment at the leading edge drives protrusion formation was recently challenged by a study reporting that β_{cyto}-actin is preferentially localized in stress fibers, while γ_{cyto}-actin primarily localized to lamellipodia in migrating fibroblasts (35). These conflicting reports are not surprising given the inherent difficulty in immunostaining actin isoforms (36). The small sequence differences between isoforms makes generating isoform specific antibodies challenging and requires establishing antibody specificity using knockout tissues, which until recently have not been available. Furthermore, some actin-based structures, such as tightly bundled actin filaments, may not allow for antibody penetration or epitope unmasking. Nonetheless, overexpression of β_{cyto}-actin in myoblasts increased areas of membrane protrusions and nearly doubled the speed of migrating cells, suggesting that β_{cyto}-actin in deed plays an important role in cell motility (37).

Studies investigating post-translational modifications of actin isoforms also implicate a specific role for β_{cyto}-actin in cell motility. While both β_{cyto}- and γ_{cyto}-actin are arginylated at the N-terminus, arginylated γ_{cyto}-actin is highly unstable and selectively degraded, thus only arginylated β_{cyto}-actin is found *in vivo* (38, 39). In fact, it was demonstrated that as much as 40% of intracellular β_{cyto}-actin is arginylated in motile

fibroblasts (38). Arginyltransferase (*Ate1)* knockout cells, which lack the enzyme necessary to carry out arginylation, failed to form normal lamellae and were migration deficient (38). Importantly, the lamellae defect was rescued by reintroduction of N-terminally arginylated β_{cyto}-actin, indicating that the defective lamellae in *Ate1* knockout cells is due specifically to a lack of arginylated β_{cyto}-actin and not any of the other ABPs known to be arginylated. The authors subsequently demonstrated a global disorganization of the cytoskeleton and reduced actin polymer levels in *Ate1* knockout cells (39). These defects were attributed to the fact that purified nonarginylated actin had altered polymerization properties, a greater tendency to aggregate, and altered interactions with several actin-binding proteins. Together, these data indicate an important function for arginylated β_{cyto}-actin in cytoskeletal maintenance and function.

The first direct evidence that cytoplasmic actins are functionally distinct came from an overexpression study in cultured cells. Mouse C2 myoblasts stably transfected with β_{cyto}-actin or γ_{cyto}-actin elicited reciprocal effects on myoblast morphology (40). Cells expressing high levels of β_{cyto}-actin displayed increases in cell surface area and thickness. In contrast, overexpression of γ_{cyto}-actin resulted in reduced cell surface area and a loss of actin stress fibers (40). While other cell types may not interpret overexpression of cytoplasmic actins in the same way, the reciprocal phenotypes nonetheless suggest that β_{cyto}- and γ_{cyto}-actin are functionally distinct.

Additional evidence for unique biological functions between the cytoplasmic actins comes from knockdown studies. In cultured cells, siRNA-induced silencing of either β_{cyto}-actin or γ_{cyto}-actin led to a halt in cell growth, suggesting that the cytoplasmic

actins are both essential genes with non-redundant functions (41). In a more recent study, it was shown that siRNA knockdown of β_{cyto}-actin led to increased cell spreading, the formation of broad protrusions at the leading edge, and reduced stress-fiber content (35). In contrast, γ_{cyto}-actin knockdown resulted in a contractile phenotype with thick actin bundles and reduced lamellipodial structures. Furthermore, siRNA-induced silencing of β_{cyto}-actin or γ_{cyto}-actin actin led to differential effects on cell motility (35). Together, these studies suggest distinct cellular roles for β_{cyto}- and γ_{cyto}-actin; however, it remains possible that the observed phenotypes are due to off-target effects of siRNA knockdown.

In addition to siRNA-mediated knockdown *in vitro*, there are two independent reports of β_{cyto}-actin knockdown *in vivo* using a targeted transgene approach (42, 43). In both studies, transgene insertion into the β_{cyto}-actin locus resulted in reduced β_{cyto}-actin expression and mice homozygous for the targeted allele were embryonic lethal by embryonic day (E) 10.5. These knockdown studies lend support to the idea that cytoplasmic actins are essential genes, each with non-overlapping functions.

In order to definitively test whether β_{cyto}- and γ_{cyto}-actin are essential genes and to help identify their distinct functions, the Ervasti laboratory generated both conditional and null alleles for the β_{cyto}- and γ_{cyto}-actin genes. Conditional knockout of γ_{cyto}-actin in skeletal muscle resulted in a progressive myopathy, characterized by muscle weakness and muscle cell death and regeneration (44). In skeletal muscle, γ_{cyto}-actin is localized to the cortical cytoskeleton and composes a very minor population of the total actin; nonetheless, γ_{cyto}-actin appears to play an important role in maintaining muscle cell structure and function. Upon generation of a null allele for γ_{cyto}-actin, it was discovered

that γ_{cyto}-actin is not essential for viability as a third of null animals (*Actg1*$^{-/-}$) could be identified at weaning (45). Nonetheless, *Actg1*$^{-/-}$ mice exhibited increased mortality and presented with a progressive hearing loss despite up-regulation of β_{cyto}-actin, indicating distinct biological functions for γ_{cyto}-actin.

The first goal of my thesis research was to identify the cause of lethality in *Actg1*$^{-/-}$ mice in an attempt to understand how γ_{cyto}-actin is functionally distinct from β_{cyto}-actin *in vivo*. To this end, I characterized the embryonic and postnatal development of *Actg1*$^{-/-}$ mice as well as assessed cell behavior of *Actg1*$^{-/-}$ primary mouse embryonic fibroblasts (MEFs). My findings from this work are described in Chapter 2. The second goal of my thesis research was to characterize β_{cyto}-actin null mice (*Actb*$^{-/-}$) and knockout MEFs to help identify specific biological functions for β_{cyto}-actin. These results are described in Chapter 3. Together, the distinct phenotypes observed in β_{cyto}-actin and γ_{cyto}-actin knockout mice and cells reveal unique biological functions for the cytoplasmic actin isoforms.

Chapter 2

Delayed Embryonic Development and Impaired Cell Growth and Survival in *Actg1* Null Mice

This chapter is unmodified from the published article:

Bunnell, T.M., and Ervasti, J.M. (2010) Delayed embryonic development and impaired cell growth and survival in Actg1 null mice. *Cytoskeleton (Hoboken)* 67, 564-572

Actins are among the most highly expressed proteins in eukaryotes and play a central role in nearly all aspects of cell biology. While the intricate process of development undoubtedly requires a properly regulated actin cytoskeleton, little is known about the contributions of different actin isoforms during embryogenesis. Of the six actin isoforms, only the two cytoplasmic actins, β_{cyto}- and γ_{cyto}-actin, are ubiquitously expressed. We found that γ_{cyto}-actin null (*Actg1*$^{-/-}$) mice were fully viable during embryonic development, but most died within 48 hours of birth due to respiratory failure and cannibalization by the parents. While no morphogenetic defects were identified, *Actg1*$^{-/-}$ mice exhibited stunted growth during embryonic and postnatal development as well as delayed cardiac outflow tract formation that resolved by birth. Using primary mouse embryonic fibroblasts, we confirm that γ_{cyto}-actin is not required for cell migration. The *Actg1*$^{-/-}$ cells, however, exhibited growth impairment and reduced cell viability, defects which perhaps contribute to the stunted growth and developmental delays observed in *Actg1*$^{-/-}$ embryos. Since the total amount of actin protein was maintained in *Actg1*$^{-/-}$ cells, our data suggests a distinct requirement for γ_{cyto}-actin in cell growth and survival.

Introduction

Actins are a major component of the cytoskeleton and play fundamental roles in most cellular processes, including muscle contraction, cell motility, cell division, cell signaling, establishment of cell polarity and maintenance of cell shape. In higher eukaryotes there are six different actin isoforms, each encoded by distinct genes: four "muscle" actins predominately expressed in striated (α_{sk} and α_{ca}) and smooth (α_{sm} and γ_{sm}) muscle and two cytoplasmic "non-muscle" actins (β_{cyto} and γ_{cyto}) which are ubiquitously expressed (13). The actin family of proteins is highly conserved, with no two isoforms differing by more than 7% of their primary amino acid sequences. Incredibly, β_{cyto}- and γ_{cyto}-actin differ at only 4 out of 375 amino acids and these small sequence differences are conserved from birds to mammals.

It has been hypothesized that the β_{cyto}- and γ_{cyto}-actin isoforms confer unique functions in certain tissues and cell types. In support of this hypothesis, β_{cyto}- and γ_{cyto}-actin mRNA and protein segregate to distinct intracellular compartments in a variety of cell types (26, 35, 46, 47). Furthermore, siRNA-induced silencing revealed β_{cyto}- and γ_{cyto}-actin as essential genes in cultured mammalian cells (41), suggesting non-redundant roles for the two non-muscle actin isoforms. In addition, hypomorphic β_{cyto}-actin mice are embryonic lethal (42, 43), indicating that β_{cyto}-actin plays an essential role during embryonic development.

During animal development, a properly regulated actin cytoskeleton is required to generate the protrusive and contractile forces necessary for morphogenetic processes. Disruption of the actin cytoskeleton, either through perturbations in actin-binding

proteins or through the use of actin-targeting drugs, leads to morphogenetic defects in several organisms, including worms, flies and mice (11, 48, 49). In addition, actin is important for completing cell division, generating cell polarity, and maintaining cell shape, all processes critical for proper embryonic development. Despite the well-recognized roles for actin during development, little is know about the individual contributions from the different actin isoforms. Indeed, β_{cyto}- and γ_{cyto}-actin isoforms exhibit differential expression patterns during development (20), suggesting that each isoform performs specific and perhaps unique functions.

We previously generated *Actg1*$^{-/-}$ mice and showed that γ_{cyto}-actin is not essential for viability, suggesting that other actin isoforms can at least partially compensate for γ_{cyto}-actin during embryonic development (45). However, only one-third of the expected number of *Actg1*$^{-/-}$ mice were found at the time of weaning (45). Therefore, we sought to characterize the embryonic and postnatal development of *Actg1*$^{-/-}$ mice to help identify processes that specifically require the γ_{cyto}-actin isoform during development. Surprisingly, *Actg1*$^{-/-}$ embryos were found at the expected Mendelian ratio throughout development and did not exhibit any gross developmental abnormalities. The observed lethality of *Actg1*$^{-/-}$ mice occurred within the first 48 hours of birth, most likely resulting from respiratory distress. This lethality could be explained by the mild developmental delays or stunted growth observed in *Actg1*$^{-/-}$ embryos. Moreover, *Actg1*$^{-/-}$ mouse embryonic fibroblasts (MEFs) exhibited growth deficiencies due to reduced cell survival. Together, these data indicate that γ_{cyto}-actin is not essential for embryonic development; however, γ_{cyto}-actin does confer advantages for growth and survival.

Materials and Methods

Animals

Generation of *Actg1*$^{+/-}$ mice was described previously (45). Animals were housed and treated in accordance with the standards set by the University of Minnesota Institutional Animal Care and Use Committee. Timed matings were carried out by housing a single *Actg1*$^{+/-}$ male with one to two *Actg1*$^{+/-}$ estrous females overnight. Vaginal plugs were checked the following morning as an indication that copulation had occurred, and male and females separated. The day a plug was detected was considered E0.5 of development. At the designated embryonic age, pregnant females were euthanized and embryos liberated from the uterine muscle and deciduum. For each embryo, gross morphology was observed, crown-rump measurements taken and yolk sac or tail tissue recovered for genotype assessment. Genotypic analysis was performed using PCR methods described previously (44). Pregnant females were observed giving birth and newborn pups were monitored. Within 3 hours of birth, lungs were dissected and examined.

Histology and immunohistochemistry

Embryonic and postnatal tissue was fixed in Bouin's fluid for 2-24 hours, depending on the size of the tissue, and stored in 70% ethanol at 4°C. Tissue was subsequently paraffin embedded and sectioned at 6 μm. Hematoxylin and eosin staining of tissue sections was carried out as described (50). Immunohistochemistry was performed using the standard Avidin-Biotin Complex technique. Tissue sections were deparaffinized in xylenes, rehydrated through a series of graded ethanol and endogenous

peroxidase activity quenched with 1.0% H_2O_2. Tissue was blocked with 2.5% goat serum and incubated with a polyclonal antibody to surfactant protein B (Abcam, ab40876) for 1.5 hours at room temperature. Sections were then incubated with a biotinylated secondary antibody (Vector Laboratories, BA1000), followed by incubation with the avidin:biotinylated enzyme complex (R.T.U. Vectastain Elite ABC Reagent, Vector Laboratories, PK7100). Immune signal was detected by exposure to the peroxidase substrate 3,3'-diaminobenzidine. Tissue sections were counterstained with hematoxylin. Histological analyses were carried out on serial sections from at least 3 different animals for each genotype/age described.

Isolation and culture of primary MEFs

Primary MEF cultures were established from E13.5 embryos. Embryos were dissected in sterile PBS and the brain, heart, liver and other visceral organs removed. The carcass was then finely minced with a razorblade and incubated in 3.0 ml of 0.25% trypsin-EDTA at 4°C overnight. Once the embryonic genotypes were determined, the minced tissue was incubated in a 37°C water bath for 30 minutes to activate the trypsin. After vigorous pipetting to break up the digested tissue, the cell suspension from each embryo was plated on two 10-cm tissue culture dishes with 10 ml of MEF culture medium (Dulbecco's modified Eagle's medium supplemented with 10% fetal bovine serum, 50 units/ml Pencillin, 50 μg/ml Streptomycin and 100 μM non-essential amino acids). The following day, cell monolayers were rinsed with sterile PBS and fresh MEF culture medium added. Cells were split at approximately 90% confluency using 0.05%

trypsin-EDTA and all analyses were carried out before the fourth passage. Cells were incubated in a humidified 37°C, 5% CO_2 incubator.

Analysis of actin composition and migration in MEFs

Cell monolayers from nearly confluent 10-cm plates were washed twice with ice-cold PBS. After addition of 300 µl of ice-cold lysis buffer (50 mM Tris-HCl, pH8.0, 150 mM NaCl, 1.0% NP-40, 0.02 mM PMSF, 0.05 µg/ml leupeptin, 5 mM EGTA), cells were collected by scraping and incubated on ice for 10 minutes. Cellular debris was removed by centrifugation and the protein concentration of the supernatant was assayed with the Bio-Rad *DC* Protein Assay Kit. Equal amounts of total protein were separated by SDS/PAGE and immunoblotted with the indicated antibodies (pan-actin, C4 (Seven Hills Bioreagents); γ_{cyto}-actin, mAb 2-4 (44); β_{cyto}-actin, AC15 (Sigma); α_{smooth}-actin, 1A4 (Sigma); $\alpha_{sarcomeric}$-actin, 5C5 (Sigma)). The ratio of G-actin versus F-actin was determined with the G-actin/F-actin *In Vivo* Assay Kit (Cytoskeleton, BK037) based on the manufacturer's protocol. Briefly, cells were lysed in F-actin stabilization buffer and cell lysates centrifuged at 100,000 x g to separate the F-actin from G-actin pool. The F-actin pellet was resuspended to the same volume as the supernatant and equal amount of samples loaded to each lane and analyzed by Western blotting using a pan-actin antibody (C4, Seven Hills Bioreagents). For the positive control sample, 1 µM phalloidin was added to the lysis buffer and incubated with wild-type cells. For both actin isoform composition and G/F-actin ratio analyses, fluorescently labeled secondary antibodies were detected and quantified from at least three separate experiments using an Odyssey infrared scanner and software (Li-Cor Biosciences, Lincoln, Nebraska, USA).

Rates of MEF cell migration were assessed using a standard scratch wound-healing assay. Cells were plated on glass-bottom dishes (MatTek Corp.) and allowed to grow to confluency. Using a yellow pipette tip, a "wound" or scratch was made across the bottom of the dish. Cell monolayers were subsequently rinsed with sterile PBS and fresh media, containing 25 mM HEPES to stabilize the pH, added to the cells. For optical clarity, a glass coverslip was used to seal the dish, creating a self-contained sterile environment. Time-lapse video of migrating cells was captured overnight at 10 min intervals using differential interference contrast (DIC) imaging on a Delta Vision personalDV (Applied Precision, Inc., Issaquah, Washington, USA) with a 40X (NA 1.35) oil objective using softWoRx 3.7.1 software. The cells were maintained at 37°C by an environmental chamber enclosing the microscope. ImageJ 1.43 software was used to measure wound area in the first frame and also in the frame just before the edges of the wound first meet (approximately the 20^{th} frame). The rate of migration was calculated as the change in wound area divided by the change in time.

Analysis of cell growth in MEFs

Cell size and viability were determined using the Vi-CELL Series Cell Viability Analyzer (Beckman Coulter, Inc.). Cell monolayers were rinsed with PBS, harvested by trypsinization and resuspended in 1.0 ml of PBS before automated analysis by the Vi-CELL. Between 200 and 3,000 cells were analyzed per sample. For the growth curve, equal numbers (10^5) of passage 1 MEFs were plated in each well of 6-well plates and counted every 24 hours in duplicate using the Vi-CELL. Cell Cycle analysis was carried out using flow cytometry to determine total DNA concentration per cell after

ethanol fixation and staining with a 20 μg/ml propidium iodide (PI) solution containing 200 μg/ml ribonuclease A. The PI fluorescent signal was collected on a BD Biosciences (San Jose, California, USA) FACSCalibur and cell cycle phases estimated using FlowJo software (Tree Star, Inc.).

Apoptosis was detected using a FITC Annexin V Apoptosis Detection Kit (BD Pharmingen). Cells were cultured for 48 hours, after which culture media was collected and cells trypsinized and counted. Cells were resuspended to the same concentration in Binding Buffer and equal volumes incubated with FITC-Annexin V and Propidium Iodide for 15 minutes at room temperature in the dark. Samples were subsequently diluted with Binding Buffer and analyzed by flow cytometry within an hour. 5 μM camptothecin was added to a plate of wild-type cells six hours before harvesting to serve as a positive control. Compensation between FL1 and FL3 was carried out using FlowJo software (Tree Star, Inc.) and data collected from singly stained samples. The Vi-Cell and FACSCalibur instruments were used at the University of Minnesota's Masonic Cancer Center Flow Cytometry Core Facility.

Results

Stunted growth and delayed cardiac development in Actg1$^{-/-}$ mice

Timed matings were established between *Actg1* heterozygous pairs and resulting *Actg1*$^{-/-}$ embryos examined. *Actg1*$^{-/-}$ embryos were morphologically similar to their wild-type counterparts throughout development (Figure 2.1A). However, they were 11% smaller in size, as measured by crown-rump length, from embryonic day (E) 10.5 to E18.5 (Figure 2.1B). *Actg1*$^{-/-}$ mice remained smaller in size during the first 3 weeks of postnatal development (Figure 2.1C) and into adulthood (45).

Histological analysis of the developing embryo revealed a delay in the development of the cardiac outflow tract in *Actg1*$^{-/-}$ embryos. During cardiac development, the proximal portion of the outflow cushions fuse and muscularize, eventually walling the aorta into the left ventricle and completing the formation of the ventricular septum (51). In wild-type embryos the aorta was observed to be exclusively in communication with the left ventricle by E13.5, however, in *Actg1*$^{-/-}$ embryos this was not observed until E14.5 of development (Figure 2.2B-C). Furthermore, in wild-type embryos but not *Actg1*$^{-/-}$ embryos, the ventricular septum was fully formed along the entire anterior-posterior axis by E14.5 (Figure 2.2D). The ventricular septum was completely formed by E18.5 in *Actg1*$^{-/-}$ embryos, indicating a developmental delay rather than a failure of cardiac outflow tract formation (Figure 2.2E).

Postnatal lethality in Actg1$^{-/-}$ mice

We previously measured sub-Mendelian ratios of *Actg1*$^{-/-}$ mice at weaning (45). To determine the time-point of lethality, timed matings were established and genotype

ratios determined at all stages of development. *Actg1*$^{-/-}$ embryos were found at the expected frequency up through E18.5 of development (Table 2.1), indicating that γ_{cyto}-actin is not required for embryonic viability. However, within 24 hours following birth the observed frequency of *Actg1*$^{-/-}$ mice was significantly less than the expected Mendelian ratio (Table 2.1). These data reveal that the observed lethality in *Actg1*$^{-/-}$ mice occurs postnatally.

Direct observation of litters born from timed matings of heterozygotes revealed that some *Actg1*$^{-/-}$ mice presented with respiratory distress at birth. Histological analysis of the developing lung did not indicate any gross morphological defects of *Actg1*$^{-/-}$ embryos (Figure 2.3A). Furthermore, the expression of surfactant protein B, a marker of lung development, was comparable between *Actg1*$^{+/-}$ and *Actg1*$^{-/-}$ mice at E18.5 (Figure 2.3A). At the time of birth, however, some *Actg1*$^{-/-}$ mice experienced difficulty breathing, which correlated with variations in the extent of saccular inflation in the lung (Figure 2.3B). These data suggest that the increased postnatal lethality of *Actg1*$^{-/-}$ mice was primarily due to respiratory distress, which in turn led to maternal cannibalism of the affected pups.

Characterization of Actg1*$^{-/-}$ *mouse embryonic fibroblasts

In order to assess cellular behavior in the absence of γ_{cyto}-actin, primary MEFs were generated from *Actg1*$^{+/+}$, *Actg1*$^{+/-}$ and *Actg1*$^{-/-}$ E13.5 embryos. We confirmed that *Actg1*$^{-/-}$ MEFs completely lacked expression of γ_{cyto}-actin protein and showed that MEFs carrying only one wild-type copy of the *Actg1* gene had reduced expression of γ_{cyto}-actin (Figure 2.4A-B). Despite the absence or reduction of γ_{cyto}-actin expression, total actin

expression levels were not different across all genotypes (Figure 2.4A-B). Total actin levels were maintained by upregulation of other actin isoforms, including the most closely related β_{cyto}-actin (Figure 2.4A-B). These data are consistent with our previous findings that total actin expression was maintained in adult *Actg1*$^{+/-}$ and *Actg1*$^{-/-}$ animals (45) and supports the existence of an actin feedback-regulatory mechanism (22, 23, 52).

We next determined whether the loss of γ_{cyto}-actin expression altered the ratio of globular (G)- to filamentous (F)-actin. It is well established that the G- to F-actin ratio is critical for proper regulation of the cytoarchitecture (6) and regulation of gene expression via serum response factor (53, 54). Using a quantitative Western blot approach, we found that the G- to F-actin ratio in MEFs was maintained in the absence of γ_{cyto}-actin expression (Figure 2.4C).

The fact that morphogenesis progresses normally in *Actg1*$^{-/-}$ embryos would suggest that γ_{cyto}-actin is not required for cell migration *in vivo*. To directly test the role of γ_{cyto}-actin during cell migration, however, we used an *in vitro* wound-healing assay. The rate of cell migration was comparable between *Actg1*$^{+/+}$ and *Actg1*$^{-/-}$ MEFs (Figure 2.5), indicating that γ_{cyto}-actin is not necessary for proper cell migration.

Given the reduced size of *Actg1*$^{-/-}$ embryos, we analyzed growth properties of MEFs and found that *Actg1*$^{-/-}$ cells exhibited growth retardation compared to control cells (Figure 2.6A). Comparable cell cycle profiles were observed between all genotypes (Figure 2.6D-E), indicating that the growth deficiency is not due to defects in the cell cycle. Furthermore, we did not observe a difference in the average cell diameter between wild-type and *Actg1*$^{-/-}$ MEFs (Figure 2.6C), indicating that cell size was not altered by

γ_{cyto}-actin ablation. The growth deficiency appears to be due to decreased cell survival, as cell viability was reduced in *Actg1*$^{-/-}$ MEFs compared to control cells (Figure 2.6B). Decreased cell survival is at least in part due to increased apoptosis (Figure 2.6F-G). As determined by an Annexin V assay, the percent of apoptotic cells increased from 5.0 ± 0.9 in wild-type MEFs to 8.6 ± 1.4 in *Actg1*$^{-/-}$ MEFs. While this increase is not statistically significant, the trend is consistent with the subtle growth deficiency observed in both *Actg1*$^{-/-}$ cells and animals.

Figure 2.1: Stunted growth in *Actg1*$^{-/-}$ mice. **A:** Shown are representative images of E18.5 *Actg1*$^{+/-}$ and *Actg1*$^{-/-}$ embryos. Scale bar: 5mm. **B:** Crown-rump length and **C:** body mass measurements during embryonic and postnatal development. *Actg1*$^{-/-}$ mice were significantly (one-way ANOVA, $p < 0.05$) smaller than *Actg1*$^{+/+}$ and *Actg1*$^{+/-}$ controls from E11.5 onward. $n \geq 4$ for each genotype/timepoint; error bars represent s.e.m.

Figure 2.1

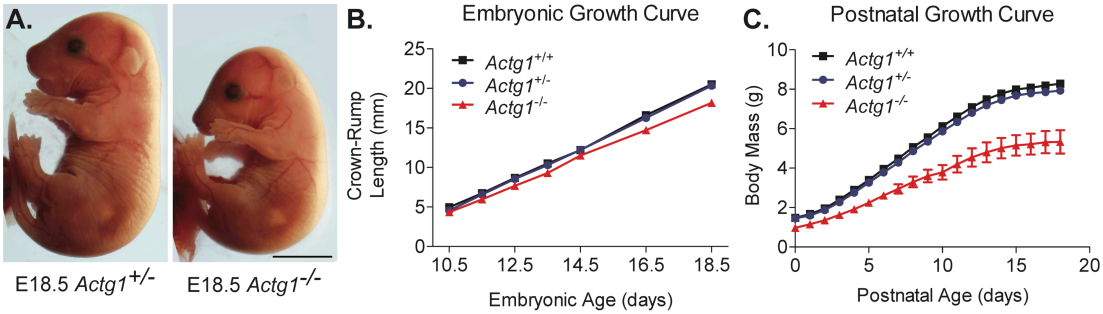
A.
E18.5 Actg1+/-
E18.5 Actg1-/-
B.
Embryonic Growth Curve
Actg1+/+
Actg1+/-
Actg1-/-
Crown-Rump Length (mm)
25
20
15
10
5
0
10.5
12.5
14.5
16.5
18.5
Embryonic Age (days)
C.
Postnatal Growth Curve
Actg1+/+
Actg1+/-
Actg1-/-
Body Mass (g)
10
8
6
4
2
0
0
5
10
15
20
Postnatal Age (days)

Figure 2.2: Delayed development of the cardiac outflow tract in *Actg1*$^{-/-}$ embryos. Shown are typical hematoxylin and eosin stained transverse sections through the embryonic heart. **A:** At E12.5 the aorta was observed to be in communication with the right ventricle in both *Actg1*$^{+/-}$ and *Actg1*$^{-/-}$ embryos. **B:** By E13.5 the aorta was observed in exclusive communication with the left ventricle in *Actg1*$^{+/-}$ embryos but remained in communication with the right ventricle in all six *Actg1*$^{-/-}$ embryos examined. **C:** By E14.5, however, the aorta had been walled into the left ventricle in six out of seven *Actg1*$^{-/-}$ embryos. **D:** At E14.5 in *Actg1*$^{+/-}$ embryos, but not in the seven *Actg1*$^{-/-}$ embryos examined (arrow), the ventricular septum was completely formed along the entire anterior-posterior axis. **E:** By E18.5 the ventricular septum had fully developed in all *Actg1*$^{-/-}$ embryos. Scale bars: 500 μm. Ao, aorta; LV, left ventricle; RV, right ventricle; VS, ventricular septum.

Figure 2.2

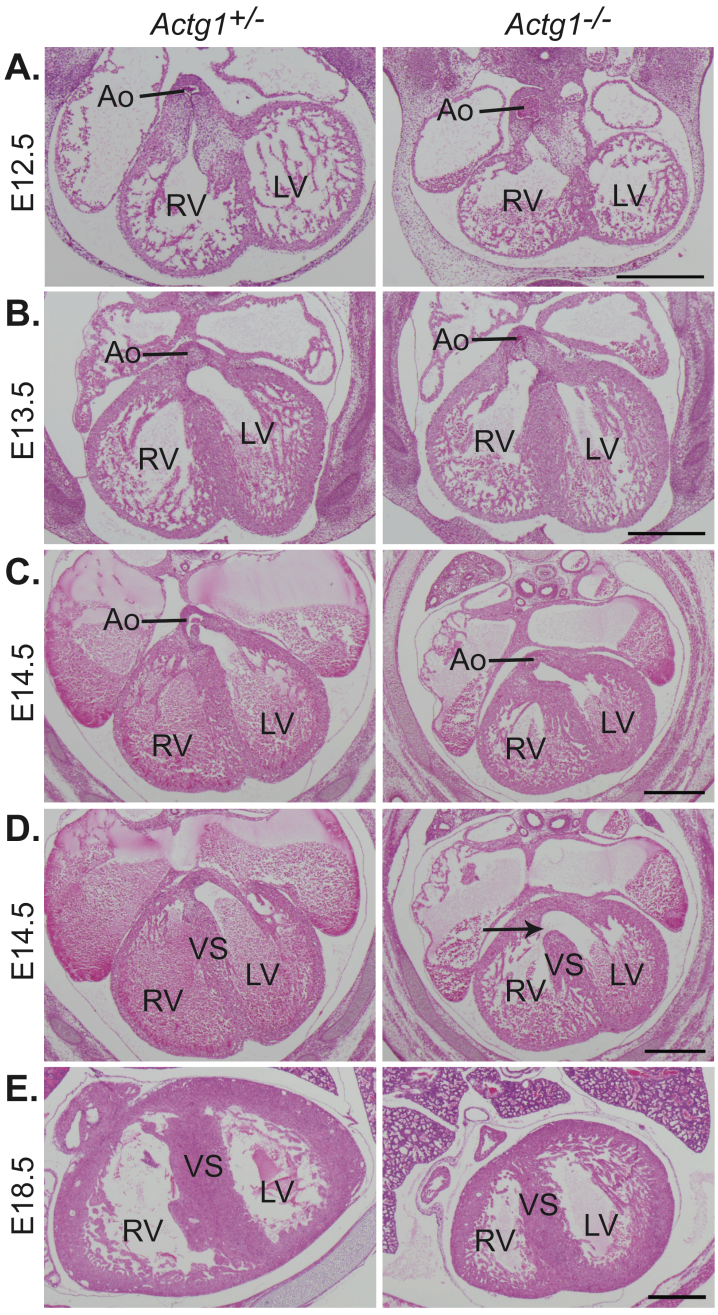

Table 2.1: Partial postnatal lethality in *Actg1*$^{-/-}$ mice

Age	n	*Actg1*$^{+/+}$	*Actg1*$^{+/-}$	*Actg1*$^{-/-}$
E10.5-14.5	434	23%	54%	23%
E16.5	86	30%	50%	20%
E18.5	113	22%	58%	20%
P0*	153	27%	63%	10%
P1*	139	27%	68%	5%

***p<0.05, Chi-square analysis**

Figure 2.3: Partially penetrant respiratory failure observed in *Actg1*$^{-/-}$ newborns. Shown are representative transverse sections of the developing lung. **A:** Hematoxylin and eosin staining of *Actg1*$^{-/-}$ lungs at E16.5 (top row) and E18.5 (middle row) revealed comparable morphology to wild-type. Immunohistochemistry using an antibody to surfactant protein B as a marker of lung development showed no differences in expression between *Actg1*$^{+/-}$ and *Actg1*$^{-/-}$ lungs at E18.5 (bottom row). **B:** In *Actg1*$^{-/-}$ lungs at P0 the extent of saccular inflation was variable and corresponds with observed variations in ability to breath at the time of birth. Scale bars: 100 μm.

Figure 2.3

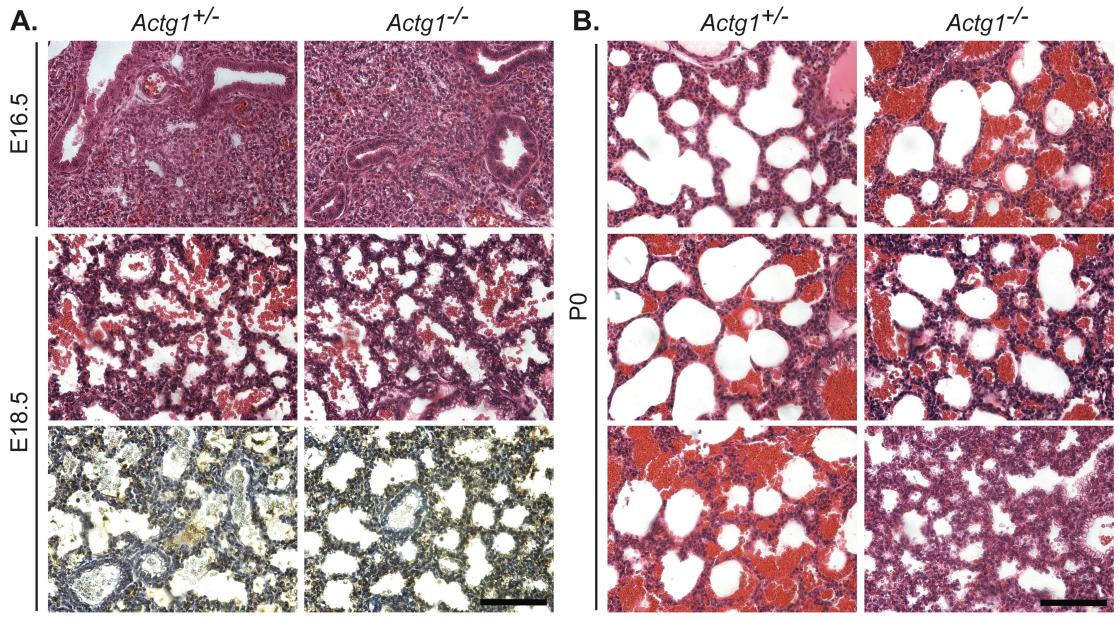

Figure 2.4: Altered actin isoform expression with no change in levels of total actin in *Actg1*$^{-/-}$ MEFs. **A:** Representative immunoblots of cell lysates from *Actg1*$^{+/+}$, *Actg1*$^{+/-}$ and *Actg1*$^{-/-}$ MEFs probed with actin isoform specific antibodies. **B:** Protein levels were quantified and are expressed relative to wild-type levels ($n \geq 3$, mean ± s.e.m.). **C:** Quantification of G- to F-actin ratios in *Actg1*$^{+/+}$, *Actg1*$^{+/-}$ and *Actg1*$^{-/-}$ MEFs ($n \geq 3$, mean ± s.e.m.).

Figure 2.4

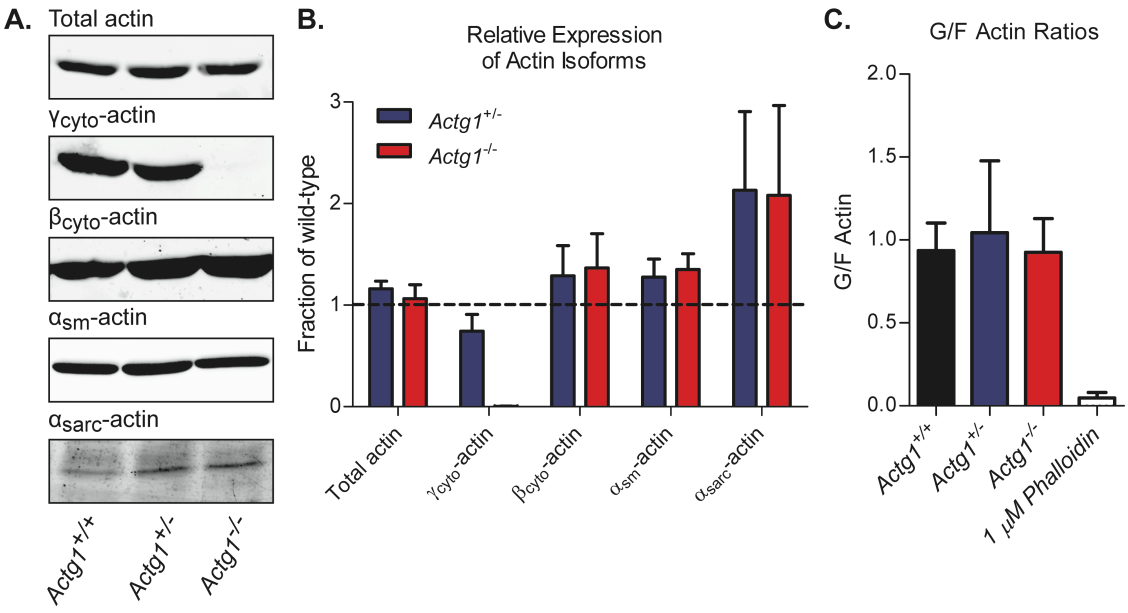
A.
Total actin
γcyto-actin
βcyto-actin
αsm-actin
αsarc-actin
Actg1+/+
Actg1+/-
Actg1-/-
B.
Relative Expression of Actin Isoforms
Actg1+/-
Actg1-/-
Fraction of wild-type
3
2
1
0
Total actin
γcyto-actin
βcyto-actin
αsm-actin
αsarc-actin
C.
G/F Actin Ratios
G/F Actin
2.0
1.5
1.0
0.5
0.0
Actg1+/+
Actg1+/-
Actg1-/-
1 μM Phalloidin

Figure 2.5: Comparable rates of cell migration between wild-type and *Actg1*$^{-/-}$ MEFs. A-B: Still images from time-lapse video microscopy showing the wound edge in yellow at time 0 and 200 minutes from both *Actg1*$^{+/+}$ and *Actg1*$^{-/-}$ MEF cultures. **C:** Rates of cell migration were calculated as the change in wound area divided by the change in time ($n \geq 3$, mean ± s.e.m.). Scale bar: 100 μm.

Figure 2.5

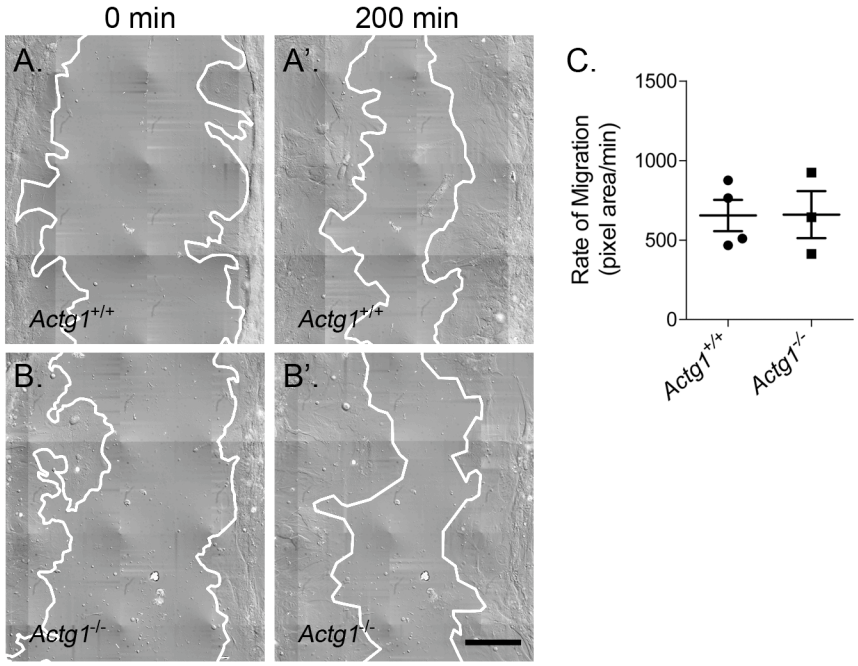
0 min
200 min
A.
A'.
B.
B'.
Actg1+/+
Actg1+/+
Actg1-/-
Actg1-/-
C.
Rate of Migration (pixel area/min)
1500
1000
500
0
Actg1+/+
Actg1-/-

Figure 2.6: Impaired growth due to decreased cell survival in *Actg1*$^{-/-}$ MEFs. A: Growth kinetics revealed impaired growth in *Actg1*$^{-/-}$ MEFs. $n = 4$ for each genotype; error bars represent s.e.m. Asterisks denote significant differences (two-way ANOVA, $p < 0.05$). **B:** Reduced cell viability in *Actg1*$^{-/-}$ MEFs as determined by an automated trypan blue exclusion assay ($n = 13$, mean ± s.e.m.). Asterisk denotes significant differences (one-way ANOVA, $p < 0.05$). **C:** Mean MEF cell size as determined by the ViCELL Series' automated contrast imaging and analysis ($n = 13$, mean ± s.e.m.). **D:** Representative cell cycle profiles. **E:** Mean percentage of cells in the G1, S, and G2 phases of the cell cycle ($n = 3$, mean ± s.e.m.). **F:** Dot plots from FITC-Annexin V flow cytometric analyses. The lower-right box represents early apoptotic cells (Annexin V-FITC Positive/ PI Negative) while the upper right box represents dead cells (Annexin V-FITC Positive/ PI Positive). **G:** Mean percentage of apoptotic cells, defined as FITC-positive and PI-negative ($n \geq 5$, mean ± s.e.m.). CPT, camptothecin.

Figure 2.6

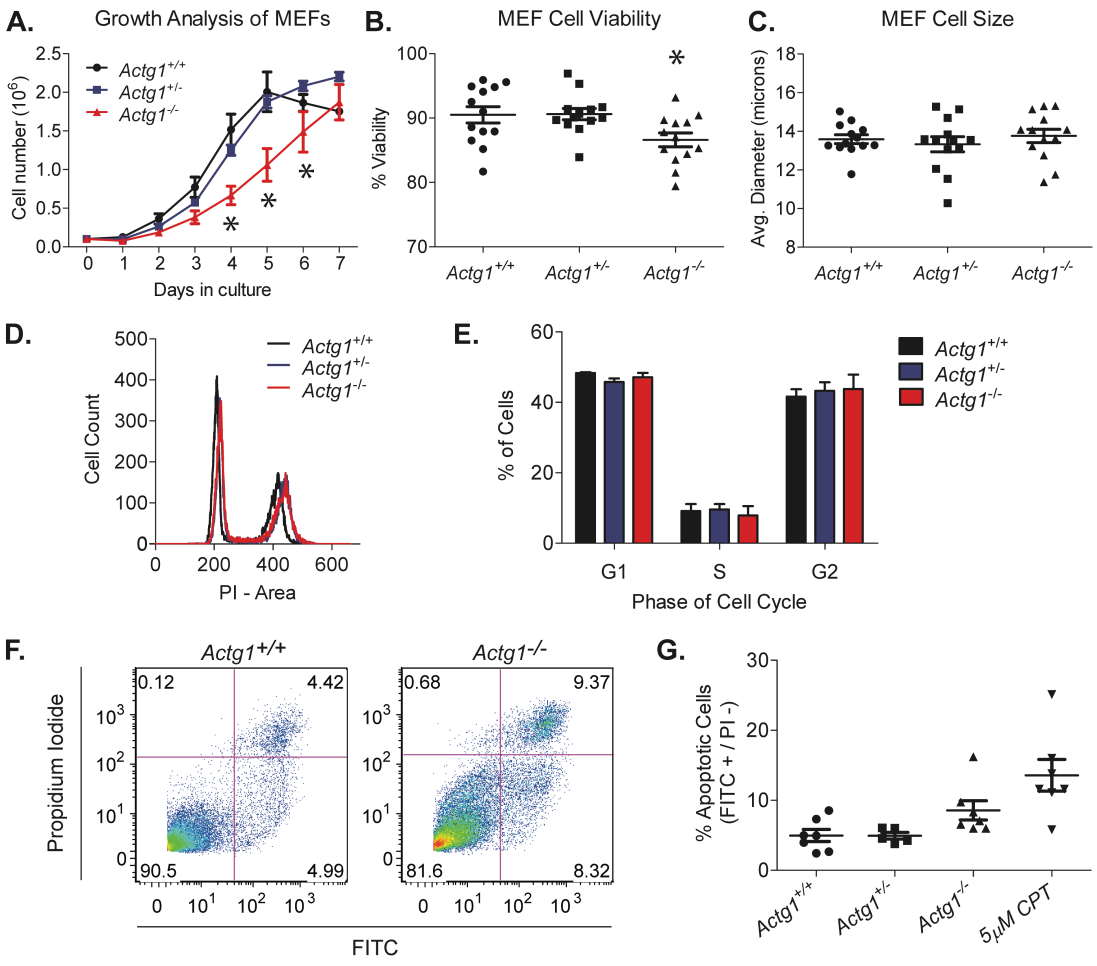
A.
Growth Analysis of MEFs
Cell number (10^6)
Days in culture
Actg1+/+
Actg1+/-
Actg1-/-
B.
MEF Cell Viability
% Viability
C.
MEF Cell Size
Avg. Diameter (microns)
D.
Cell Count
PI - Area
E.
% of Cells
G1
S
G2
Phase of Cell Cycle
F.
Actg1+/+
Actg1-/-
Propidium Iodide
FITC
0.12
4.42
90.5
4.99
0.68
9.37
81.6
8.32
G.
% Apoptotic Cells (FITC + / PI -)
5μM CPT

Discussion

The high degree of conservation of small sequence differences between the cytoplasmic actins has suggested distinct requirements for the two isoforms. While γ_{cyto}-actin is not absolutely essential for viability (45), we show that γ_{cyto}-actin clearly confers advantages during development, as *Actg1*$^{-/-}$ animals were smaller in size and exhibited a delay in the development of the cardiac outflow tract. Furthermore, most *Actg1*$^{-/-}$ mice died during the postnatal period, likely due to respiratory distress and subsequent cannibalization by the parents. In conjunction with our *in vivo* results, we observed reduced growth kinetics in *Actg1*$^{-/-}$ primary MEFs as a result of decreased cell survival. Taken together, our data illustrates that γ_{cyto}-actin provides a distinct advantage for growth and survival both *in vitro* and *in vivo*.

We provide evidence that increased apoptosis can at least partially account for the reduced cell survival of *Actg1*$^{-/-}$ MEFs. Many studies have demonstrated that actin plays a key role in the regulation of apoptosis (55). While actin has been linked to multiple stages of the apoptotic pathway, the precise mechanism by which actin regulates apoptosis remains elusive. A greater understanding of the exact function of actin in programmed cell death will be necessary to elucidate the mechanism whereby the loss of γ_{cyto}-actin leads to increased apoptosis. Nonetheless, elevated levels of apoptosis provide a possible explanation for the reduced body size and delayed development in *Actg1*$^{-/-}$ embryos.

Until recently, β_{cyto}-actin was thought to be the actin isoform critical for cell motility. A range of studies have demonstrated that β_{cyto}-actin is enriched at the leading

edge of migrating cells, while γ_{cyto}-actin is more uniformly distributed throughout the cell (24-27, 56). Furthermore, β_{cyto}-actin overexpression leads to increased areas of protrusion and cell migration (37). In contrast, Dugina et al. (35) recently reported that γ_{cyto}-actin is the predominate species at lamellipodial protrusions and that a modest decrease in γ_{cyto}-actin induced by siRNA knockdown caused severe cell migration defects. Our *in vivo* and *in vitro* results clearly demonstrate that γ_{cyto}-actin is not required for cell migration and is consistent with evidence that β_{cyto}-actin is the predominant isoform that drives cell migration.

It has long been thought that the strict evolutionary conservation of cytoplasmic actin coding sequences confers distinct and critical functions for β_{cyto} and γ_{cyto}-actin. We previously reported a progressive hearing loss in *Actg1*$^{-/-}$ adult mice (45) that is similar to human patients with γ_{cyto}-actin point mutations (57, 58). The fact that total actin levels are maintained in *Actg1*$^{-/-}$ mouse tissues (45) and MEFs suggests that the phenotypes observed in *Actg1*$^{-/-}$ mice and cells are due to unique functions for γ_{cyto}-actin. The four amino acid differences between β_{cyto} and γ_{cyto}-actin are located at the N-terminus, where actin associated proteins are known to bind; however, there is limited evidence for actin isoform specific binding proteins (59, 60). Alternatively, differential expression patterns could account for the lack of complete compensation by alternate actin isoforms in *Actg1*$^{-/-}$ animals. The expression patterns of actin isoforms are known to be temporally and spatially regulated during development (20). A new mouse model will be necessary to test whether transgenic expression of β_{cyto}-actin, under the same regulatory control as γ_{cyto}-actin, can rescue the *Actg1*$^{-/-}$ phenotype.

Biochemical differences between β_{cyto} and γ_{cyto}-actin could also account for subtle cellular phenotypes. Bergeron et al. (61) recently reported that γ_{cyto}-actin filaments are less dynamic than β_{cyto}-actin filaments, with γ_{cyto}-actin polymerizing more slowly and exhibiting enhanced filament stability. These intrinsic biochemical differences likely contribute to the distinct requirements of the two cytoplasmic actins.

Acknowledgements

We thank K. Sonnemann and B. Perrin for valuable advice throughout the project, as well as K. Downs for technical guidance. This work was supported by National Institutes of Health grant AR049899 to J.M.E.

Chapter 3

β_{cyto}-Actin is an Essential Gene Required for Embryogenesis and Cell Migration

Of the six different actin isoforms, only β_{cyto}- and γ_{cyto}-actin are ubiquitously expressed. While together β_{cyto}- and γ_{cyto}-actin undoubtedly play a critical role in most cellular processes, the unique contribution of each isoform is only just beginning to be understood. We generated a β_{cyto}-actin knockout mouse (*Actb*$^{-/-}$) and found the gene deletion to be early embryonic lethal, indicating that β_{cyto}-actin is an essential gene required for embryogenesis. The lethality in *Actb*$^{-/-}$ mice is likely due to defects in cell growth and migration as these processes were severely impaired in β_{cyto}-actin knockout primary mouse embryonic fibroblasts (MEFs). β_{cyto}-Actin knockout MEFs exhibited a zero growth rate along with increased levels of apoptosis and a higher frequency of multinucleate cells. In addition, we observed significant migration defects during random cell migration in β_{cyto}-actin knockout MEFs but not γ_{cyto}-actin null (*Actg1*$^{-/-}$) MEFs. Migration defects in β_{cyto}-actin knockout cells were associated with increased stress fibers and reduced leading edge dynamics, defects not observed in *Actg1*$^{-/-}$ cells. These distinct phenotypes occurred despite our observations that β_{cyto}- and γ_{cyto}-actin completely colocalize in wild-type MEFs, suggesting that biochemical differences between the two isoforms rather than localization differences confer unique biological functions.

Introduction

Actin is important for providing cells with internal mechanical support, tracks for myosin motor proteins, and driving forces for cell movement. These functions are attributed to the ability of actin to form stiff filaments that can rapidly assemble and disassemble according to the needs of the cell. There exist six different, but highly conserved actin isoforms in vertebrates (reviewed in (13)). Four of these isoforms are expressed primarily in striated (α_{sk} and α_{ca}) and smooth (α_{sm} and γ_{sm}) muscle cells, while the two cytoplasmic actins (β_{cyto} and γ_{cyto}) are ubiquitously expressed. Each isoform is the product of a separate gene, with *Actb* and *Actg1* encoding for β_{cyto}- and γ_{cyto}-actin respectively. Conserved from birds to mammals, β_{cyto}-actin and γ_{cyto}-actin differ at only 4 biochemically similar amino acid residues, suggesting evolutionary pressure to maintain these small sequence differences. In fact, it was recently demonstrated that these amino acid differences confer unique biochemical properties between the two isoforms (61). How these distinct properties translate to functional specificity within the cell, however, remains elusive.

It has long been thought that the β_{cyto}- and γ_{cyto}-actin isoforms confer unique biological functions. This is strongly supported by the observation that β_{cyto}- and γ_{cyto}-actin deficient mice have distinct phenotypes. It was first reported that mice hypomorphic for β_{cyto}-actin die during development of uncharacterized defects (42, 43). In contrast, γ_{cyto}-actin null (*Actg1*$^{-/-}$) mice are viable, however, they present with some notable phenotypes (45). Specifically, γ_{cyto}-actin knockout resulted in developmental delays, reduced postnatal and adult survival, and progressive myopathy (44, 45, 62).

Additionally, β_{cyto}- and γ_{cyto}-actin deficient hair cells display different patterns of progressive hearing loss and distinct stereocilia pathologies (63). The fact that total actin expression levels are maintained in *Actg1*$^{-/-}$ tissues suggests that these phenotypes are due to changes in actin isoform composition and not the concentration of total actin.

A dynamic actin cytoskeleton is essential for cell motility. Specifically, actin polymerization at the leading edge provides the protrusive forces that drive membrane extension, while disassembly of older filaments a short distance behind the leading edge replenishes the pool of actin monomers (6). We previously demonstrated that γ_{cyto}-actin is not required for cell motility (62), which is consistent with evidence that β_{cyto}-actin is the predominant isoform driving cell migration. First, one study demonstrated overexpression of β_{cyto}-actin leads to an increase in membrane protrusions and cell migration (37). Additionally, several studies have shown that β_{cyto}-actin is enriched at the leading edge of migrating cells, while γ_{cyto}-actin is more uniformly distributed throughout the cell (24-27, 56). Preferential targeting of β_{cyto}-actin to the leading edge is thought to occur via a zipcode binding sequence found in β_{cyto}-actin but not γ_{cyto}-actin mRNA. This zipcode sequence is recognized by zipcode binding protein 1 (ZBP1), which mediates the asymmetric transport and translation of β_{cyto}-actin mRNA (64). Lastly, it has been shown that β_{cyto}-actin but not γ_{cyto}-actin is N-terminally arginylated *in vivo* (39), which in turn regulates lamella formation in motile cells (38). It has thus been proposed that in combination with preferential targeting of β_{cyto}-actin to the leading edge, arginylation of β_{cyto}-actin actin regulates formation of the distinctive actin network in lamella and thus facilitates membrane extension during cell migration (65). Despite strong evidence that

β_{cyto}-actin plays a specific role in cell migration, the effects of a targeted deletion of *Actb* on cell motility has never been examined.

Cell motility is an essential process during the entire life span of vertebrates but is especially critical during many stages of development. In addition to migration, embryonic development requires a properly regulated actin cytoskeleton for completing cell division, generating cell polarity, and directing cell shape changes. We've previously shown that γ_{cyto}-actin is not essential for embryonic development, suggesting that other actin isoforms can compensate for the loss of γ_{cyto}-actin (45, 62). Here, we sought to address whether β_{cyto}-actin is uniquely required for embryonic development by generating a whole-body β_{cyto}-actin knockout mouse (*Actb*$^{-/-}$). We found *Actb*$^{-/-}$ mice to be early embryonic lethal, demonstrating that β_{cyto}-actin is essential for embryonic development. This finding correlated with severe growth impairment and considerable migration defects in β_{cyto}-actin knockout primary mouse embryonic fibroblasts (MEFs). Migration defects were associated with increased stress fibers and reduced membrane protrusion dynamics, despite the observation that β_{cyto}- and γ_{cyto}-actin colocalize in wild-type cells. In contrast to β_{cyto}-actin knockout MEFs, cell migration and membrane protrusion dynamics were normal in γ_{cyto}-actin null MEFs. From these results we conclude that β_{cyto}-actin but not γ_{cyto}-actin is an essential gene specifically required for cell migration.

Materials and Methods

Animals

Animals were housed and treated in accordance with the standards set by the University of Minnesota Institutional Animal Care and Use Committee. The floxed *Actb* allele was described previously (63). Mice carrying the floxed allele were crossed to mice expressing EIIa-cre (66) to generate $Actb^{+/-}$ mice. $Actb^{+/-}$ mice were backcrossed to C57Bl/6 for 10 generations before intercross breedings were arranged. $CAGGCre\text{-}ER^{TM}$ transgenic mice (67) (obtained from Jackson labs on the C57Bl/6 background) and $Actg1^{+/-}$ mice (45) have been previously described. Genotypic analyses were performed by standard PCR methods.

Timed matings were established between heterozygous pairs and vaginal plugs checked in the morning as an indication that copulation had occurred. The day a plug was detected was considered E0.5 of development. At the designated embryonic age, pregnant females were euthanized and embryos liberated from the uterine muscle and deciduum. Yolk sac tissue was recovered from later stage embryos and standard DNA isolation and PCR methods used for genotype assessment. At E7.5-8.5 the entire embryonic tissue was placed in 10 µl lysis buffer (500 mM KCl, 100 mM Tris-HCl, 0.45% NP-40, 0.45% Tween 20, and 500 µg/ml proteinase K) and incubated at 55°C for 3 hours. Samples were boiled 10 minutes to inactivate the proteinase K and used directly for PCR.

Cell culture and treatment

Primary MEF cultures were established from E13.5 embryos as described (62). Cells from each embryo were grown to confluency on a 10-cm plate and subsequently frozen at $1x10^6$ cells/ml in MEF freezing medium (Dulbecco's Modified Eagle's Medium supplemented with 30% fetal bovine serum and 10% dimethylsulfoxide) until ready for use. Cells were then thawed and plated with MEF culture medium (Dulbecco's Modified Eagle's Medium supplemented with 10% fetal bovine serum, 50 μg/ml Streptomycin, 50 units/ml Penicillin and 100μM nonessential amino acids). The following day, homozygous *Actb* floxed ($Actb^{L/L}$) and $Actb^{L/L}$ $CAGGCre\text{-}ER^{TM}$ cells were dosed with 1 μM tamoxifen (Sigma) to initiate recombination. After 3 consecutive days of tamoxifen treatment, MEF cultures were maintained for an additional 4 days to allow for protein turnover. Cells were passaged by trypsinization (0.05% trypsin-EDTA) on a consistent basis and all analyses were carried out at the third passage. Cells were incubated in a humidified 37°C, 5% CO_2 incubator.

Immunoblot analyses

Tissues were collected from 9-week-old $Actb^{+/+}$ and $Actb^{+/-}$ animals, snap frozen in liquid nitrogen, and ground into powder using a liquid nitrogen-cooled mortar and pestle. Pulverized tissue was boiled in 1% SDS, 5 mM EGTA, and protease inhibitors for 2 minutes followed by brief centrifugation to pellet out insoluble material. MEF cell lysates were prepared as previously described (62). Protein concentration of tissue and cell lysates was determined using the Bio-Rad DC Protein Assay Kit. Equal amounts of total protein were separated by SDS/PAGE and immunoblotted with the following

antibodies: pan-actin (C4, Seven Hills Bioreagents), β_{cyto}-actin (AC15, Sigma), γ_{cyto}-actin (mAb 2-4, (44)), α_{smooth}-actin (1A4, Sigma). Fluorescently labeled secondary antibodies were detected and quantified using the Odyssey Infrared Imaging System (LI-COR Biosciences, Lincoln, NE).

Immunofluorescent microscopy

MEFs were plated on glass coverslips pre-coated with 5 μg/ml fibronectin (BD Biosciences) and cultured for 3 hours or overnight as indicated. Cells were fixed in 4% paraformaldehyde (Electron Microscopy Sciences) in PBS for 10 min at 37°C and permeabilized with 0.2% Triton X-100 in PBS for 10 min at room temperature. Treatment with cold methanol at -20°C for 10 minutes was necessary for use with β_{cyto}- and γ_{cyto}-actin antibodies. Cells were blocked for 1 hour in 3% bovine serum albumin and incubated with the actin-isoform specific antibodies β_{cyto}-actin (FITC conjugated AC15, Abcam) and γ_{cyto}-actin (Alexa-568 conjugated mAb 1-37, (63)). F-actin was labeled with Phalloidin-Alexa 488 (Invitrogen). Coverslips were mounted using ProLong Gold antifade reagent with DAPI (Invitrogen). Images were acquired using a 20x (NA 0.75), 40x oil (NA 1.35), or 100x oil (NA 1.40) objective on a Delta Vision personalDV microscope using softWoRx 3.7.1 software (Applied Precision). Stacks of images were collected at 0.20 μm intervals, deconvolved using Resolve3d software (Applied Precision), and processed using ImageJ 1.43 software.

G/F-actin ratios

G- to F-actin ratios were determined using a commercial kit (Cytoskeleton) as previously described (62).

Analysis of cell growth

To generate the growth curve, equal numbers (10^5) of MEFs were plated in each well of 6-well plates and cells counted every 24 hours in duplicate using a hemocytometer. On the final day of the growth curve cells were replated on fibronectin-coated coverslips and stained with phalloidin and DAPI as described above to quantify the percent multinucleate cells. Cellular DNA content was analyzed by flow cytometry after staining ethanol-fixed cells with a 20 μg/ml propidium iodide solution containing 200 μg/ml ribonuclease A. Apoptosis was detected by flow cytometry using a FITC Annexin V Apoptosis Detection Kit (BD Pharmingen) as previously described (62). Fluorescent signals were collected on a BD Biosciences FACSCalibur flow cytometer at the University of Minnesota's Masonic Cancer Center Flow Cytometry Core Facility and data analysis was carried out using FlowJo software (Tree Star).

Live-cell imaging

Live-cell imaging was performed on a Delta Vision personalDV (Applied Precision) using differential interference contrast (DIC) imaging with a 40x (NA 1.35) oil objective or by phase contrast illumination with a 10x (NA 0.25) objective. Cells were plated at a density of 2.0 x 10^3 cells/cm^2 on glass-bottom dishes (MatTek Corp.) pre-coated with 5 μg/ml fibronectin (BD Biosciences) and allowed to adhere for 3 hours before the start of imaging. For optical clarity, the dish was sealed with vacuum grease and a glass coverslip. MEF culture media containing 25 mM HEPES was used to stabilize the pH and the cells were maintained at 37°C by an environmental chamber

enclosing the microscope. For random migration, images were captured at 10-minute intervals and cells tracked using the Manual Tracking plugin for ImageJ software. Cells that divided or made contact with other cells during the experiment were not used for data analysis. Velocity was calculated as the total track distance divided by the total time (240 minutes) and directionality (D/T) calculated as the linear distance (D) divided by the total track distance (T). More than 85 cells from at least 3 independent experiments were analyzed. For kymography, cells were imaged for 10 minutes at 3-second intervals using the 40x objective. Kymographs were generated and analyzed as previously described (68) using the ImageJ Kymograph plugin. At least 74 protrusion and 54 retraction events were quantified from between 15 and 40 lamellipodial protrusions for each genotype. Only lamellipodia that protruded consistently during the entire 10-minute movie were analyzed.

Statistical analysis

Unless otherwise noted, comparisons between 2 groups were performed by an unpaired t test. Comparisons between more than 2 groups were performed by one-way ANOVA followed by Tukey's post hoc test. A value of $p < 0.05$ was considered statistically significant.

Results

β_{cyto}-Actin is essential for in vivo survival

To determine the requirement for β_{cyto}-actin *in vivo* we generated a null allele by deleting exons 2 and 3 of the *Actb* locus, thereby removing the translational start site. Mice heterozygous for the null allele ($Actb^{+/-}$) were hypomorphic, expressing 18-33% less β_{cyto}-actin compared to $Actb^{+/+}$ mice depending on the tissue analyzed (Figure 3.1A-B). While compensatory up-regulation of other actin isoforms was observed in all tissues, total actin expression was only restored in the liver and kidneys but not in the brain or lungs (Figure 3.1A-B). Despite just a modest decrease in β_{cyto}-actin, approximately 30% of $Actb^{+/-}$ mice died between 5 and 18 weeks of age (Figure 3.1C), primarily due to hydrocephalus resulting from unknown causes. Homozygous deletion of *Actb* resulted in embryonic lethality, as evidenced by the fact that no $Actb^{-/-}$ mice were live born. Genotyping of embryos at various gestational ages from heterozygous crosses revealed less than expected frequencies of $Actb^{-/-}$ mice as early as E7.5 with no $Actb^{-/-}$ mice surviving beyond E8.5 (Table 3.1). Already by E7.5 $Actb^{-/-}$ embryos were considerably smaller than their wild-type counterparts (Figure 3.1D). The early embryonic lethality of $Actb^{-/-}$ mice indicates that β_{cyto}-actin is an essential gene that plays a critical role during early stages of development.

Establishing primary cultures of β_{cyto}-actin knockout MEFs

To assess whether there is a unique function for β_{cyto}-actin in cell behavior, we established a system for knocking out β_{cyto}-actin in primary MEFs. Mice carrying floxed alleles of *Actb* ($Actb^{L/L}$; (63)) were crossed to the CAGG-CreER^{TM} transgenic line, which

express a tamoxifen-inducible Cre recombinase under the control of a ubiquitous promoter (67). Primary MEFs were generated from *Actb*$^{L/L}$ and *Actb*$^{L/L}$ *CAGG-CreER*^{TM} E13.5 embryos and treated with tamoxifen for 3 consecutive days to induce recombination in Cre expressing cells. While shorter treatment times with tamoxifen were also tested, we found it resulted in less efficient knockout. After tamoxifen treatment, cells were cultured for an additional 4 days in order to allow for protein turnover. Immunofluorescence with a β_{cyto}-actin specific antibody demonstrated a lack of β_{cyto}-actin expression in more than 95% of *Actb*$^{L/L}$ *CAGG-CreER*^{TM} (herein referred to as *Actb*$^{L/L}$ *Cre*) cells (Figure 3.2A-B). The small population of β_{cyto}-actin positive cells likely represents those that did not undergo recombination. Efficient ablation of β_{cyto}-actin was further confirmed by western blot analysis, which revealed total β_{cyto}-actin protein levels in *Actb*$^{L/L}$ *Cre* cells to be less than 5% of *Actb*$^{L/L}$ cells (Figure 3.2C-D). As a result of compensatory up-regulation of other actin isoforms, total actin expression was maintained in *Actb*$^{L/L}$ *Cre* cells (Figure 3.2C-D). Importantly, this data indicates that any phenotypes resulting from knockout of β_{cyto}-actin are due to changes in actin isoform composition and not the concentration of actin.

β_{cyto}-Actin and γ_{cyto}-actin colocalize in MEFs

Many studies have reported distinct localization patterns of β_{cyto}- and γ_{cyto}-actin in migrating cells (24-27, 35, 56); however, there are discrepancies between studies regarding the precise localization of the two isoforms. Using our β_{cyto}-actin knockout cells and γ_{cyto}-actin null (*Actg1*$^{-/-}$) cells (62), we were able to verify isoform specificity of β_{cyto}- and γ_{cyto}-actin antibodies (Figure 3.3A-B). Simultaneous labeling of wild-type

MEFs with isoform-specific antibodies demonstrated colocalization of β_{cyto}- and γ_{cyto}-actin in all actin-containing structures at the resolution of light microscopy (Figure 3.3C-D). Both isoforms were localized to stress fibers, lamellipodial protrusions, and membrane ruffles, therefore we did not detect differential localization of β_{cyto}- and γ_{cyto}-actin in our primary MEFs under the described culture conditions.

β_{cyto}-Actin knockout leads to decreased G/F-actin ratios

We observed more prominent stress fibers in *Actb*$^{L/L}$ *Cre* cells compared to wild-type cells (Figure 3.3B-C), therefore we sought to assess the ratio of globular (G)- to filamentous (F)-actin. We used high-speed centrifugation to separate the G- and F-actin pools from cell lysates, followed by quantitative Western blot analysis using a pan-actin antibody (Figure 3.4A-B). The ratio of G- to F-actin was significantly decreased in *Actb*$^{L/L}$ *Cre* cells, thereby confirming increased cellular F-actin content in the absence of β_{cyto}-actin (Figure 3.4B).

β_{cyto}-Actin knockout MEFs are growth impaired

Reduced cell survival was previously observed in *Actg1*$^{-/-}$ MEFs (62); therefore we assessed the growth properties of β_{cyto}-actin knockout cells. Analysis of growth kinetics revealed *Actb*$^{L/L}$ *Cre* cells to be severely growth impaired (Figure 3.4C). While *Actb*$^{L/L}$ cells exhibited a typical growth pattern, *Actb*$^{L/L}$ *Cre* cells failed to increase in number over a 7-day period (Figure 3.4C). Contributing to this zero growth rate was increased apoptosis, as the percent of apoptotic cells was 13.1% in *Actb*$^{L/L}$ *Cre* MEFs compared to 3.2% in control MEFs (Figure 3.4D-E). Multinucleate cells were also significantly increased in *Actb*$^{L/L}$ *Cre* MEFs, but not in *Actg1*$^{-/-}$ MEFs (Figure 3.4F). This

result was further corroborated by flow cytometric analysis of DNA content, which revealed a larger percentage of cells with 4N DNA content in *Actb*$^{L/L}$ *Cre* cells compared to *Actb*$^{L/L}$ cells (Figure 3.4G). Due to the inherent difficulty in synchronizing primary cells, we were unable to further analyze the cytokinesis defect in *Actb*$^{L/L}$ *Cre* MEFs; nonetheless these data suggest that cytokinesis may specifically require β_{cyto}-actin.

Migration defects in the absence of β_{cyto}-actin

γ_{cyto}-Actin was previously shown to be dispensable for migration *in vivo* and *in vitro* (62); therefore we sought to investigate whether β_{cyto}-actin might be important for cell migration. Given the growth impairment of *Actb*$^{L/L}$ *Cre* cells, confluent cell monolayers for wound healing assays were difficult to achieve, therefore we used a random cell migration assay. Individual cells were tracked at 10-minute intervals for 4 hours and the velocity of migration and directional persistence calculated. A clear difference in the migratory ability of *Actb*$^{L/L}$ *Cre* cells was observed (Figure 3.5A). In contrast to *Actg1*$^{-/-}$ cells, migration velocity was significantly decreased in *Actb*$^{L/L}$ *Cre* cells compared to controls (Figure 3.5B). Directional persistence was comparable across all genotypes (Figure 3.5C).

It has been suggested that β_{cyto}-actin is the major actin isoform driving membrane protrusions at the leading edge of migrating cells. To test this idea we analyzed kymographs from active lamellipodia of control, *Actb*$^{L/L}$ *Cre*, and *Actg1*$^{-/-}$ cells in order to assess leading edge dynamics in the absence of β_{cyto}-actin or γ_{cyto}-actin (Figure 3.5D-G). Kymographs generated from *Actb*$^{L/L}$ *Cre* lamellipodia revealed that the frequency of protrusion and retraction events was significantly decreased compared to control

lamellipodia (Figure 3.5F-G). Correspondingly, the average duration of protrusive events was increased in *Actb*$^{L/L}$ *Cre* cells (Figure 3.5F). Most notable, however, is that protrusion velocity was significantly decreased in lamellipodia from *Actb*$^{L/L}$ *Cre* cells (Figure 3.5F). The duration and velocity of retraction events was not affected by the loss of β_{cyto}-actin (Figure 3.5G). In contrast to *Actb*$^{L/L}$ *Cre* cells, leading edge dynamics in *Actg1*$^{-/-}$ cells was comparable to controls (Figure 3.5F-G). Together, these data indicate a specific function for β_{cyto}-actin in membrane protrusion dynamics during cell migration.

Figure 3.1: *In vivo* characterization of β_{cyto}-actin deficiency. **A:** Representative immunoblots of SDS extracts from *Actb*$^{+/+}$ and *Actb*$^{+/-}$ adult brain and kidney tissue probed with antibodies specific for β_{cyto}-actin, γ_{cyto}-actin, α_{sm}-actin, or pan-actin. **B:** Protein levels were quantified from brain, liver, kidney and lung tissues. Bar graphs represent relative expression levels in *Actb*$^{+/-}$ tissues as compared to *Actb*$^{+/+}$ levels (n = 3, mean ± s.e.m.). **C:** Kaplan-Meier survival curve of *Actb*$^{+/+}$ and *Actb*$^{+/-}$ mice from 0 to 320 days of age. Tick marks represent censored animals. Survival curves are significantly different ($p < 0.0001$, log-rank test; $n \geq 62$ for each genotype). **D:** Representative images of E7.5 *Actb*$^{+/+}$ and *Actb*$^{-/-}$ embryos. Scale bar: 200 μm.

Figure 3.1

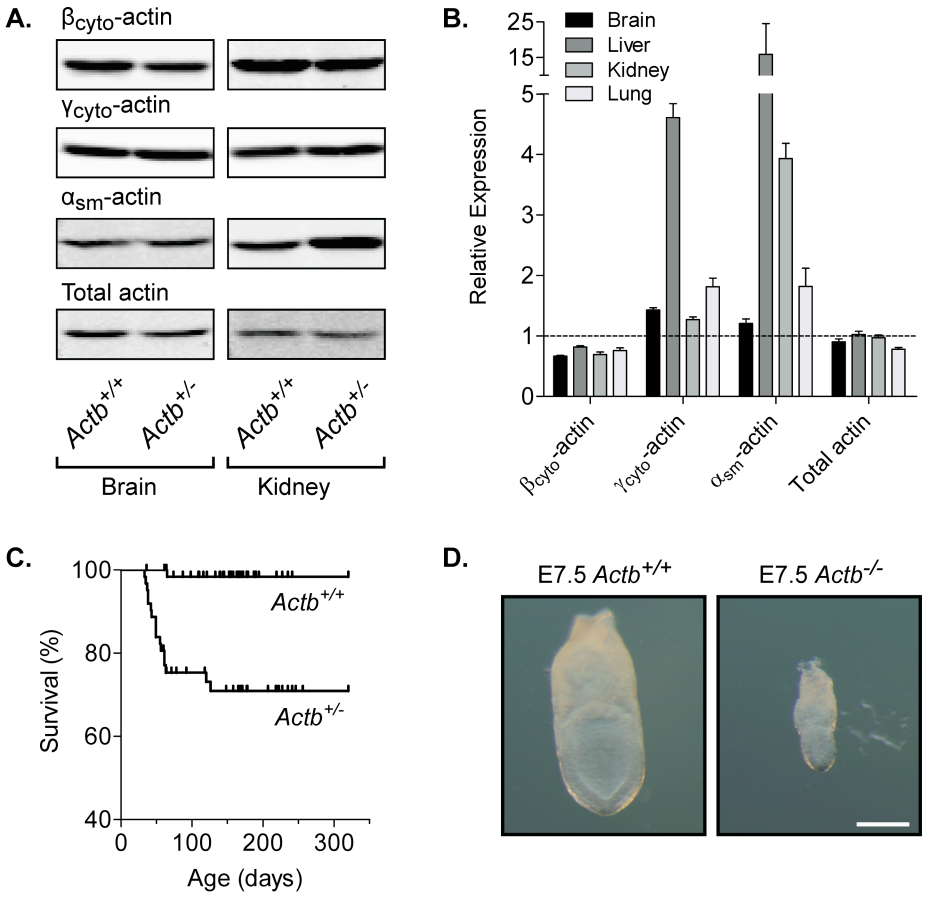
A.
βcyto-actin
γcyto-actin
αsm-actin
Total actin
Actb+/+
Actb+/-
Actb+/+
Actb+/-
Brain
Kidney
B.
Brain
Liver
Kidney
Lung
Relative Expression
25
15
5
4
3
2
1
0
βcyto-actin
γcyto-actin
αsm-actin
Total actin
C.
Survival (%)
100
80
60
40
Actb+/+
Actb+/-
0
100
200
300
Age (days)
D.
E7.5 Actb+/+
E7.5 Actb-/-

Table 3.1: Early embryonic lethality in *Actb*$^{-/-}$ mice

Age	n	*Actb*$^{+/+}$	*Actb*$^{+/-}$	*Actb*$^{-/-}$
E7.5*	51	37%	57%	6%
E8.5*	58	36%	57%	7%
E9.5*	26	31%	69%	0%
E13.5*	27	44%	56%	0%

***p<0.05, Chi-square analysis**

Figure 3.2: Efficient knockout of β_{cyto}-actin in MEFs. A-B: Representative images of *Actb*$^{L/L}$ (A) and *Actb*$^{L/L}$ *Cre* (B) MEFs cultured overnight and co-stained with antibodies to β_{cyto}-actin (green) and γ_{cyto}-actin (red). **C:** Representative immunoblots of cell lysates from *Actb*$^{L/L}$ and *Actb*$^{L/L}$ *Cre* MEFs probed with pan actin or actin isoform specific antibodies. **D:** Expression levels in *Actb*$^{L/L}$ *Cre* cells relative to *Actb*$^{L/L}$ cells (n = 5, mean ± s.e.m.).

Figure 3.2

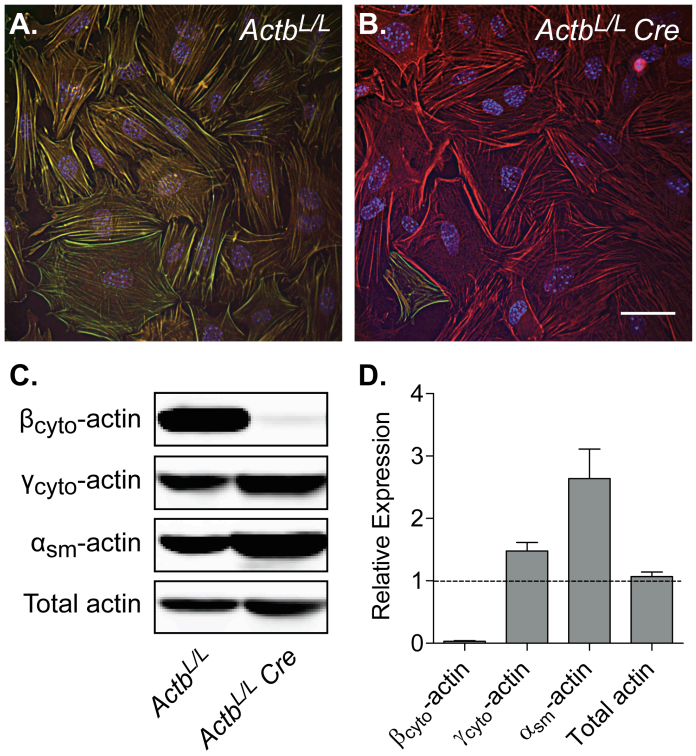
A.
Actb L/L
B.
Actb L/L Cre
C.
βcyto-actin
γcyto-actin
αsm-actin
Total actin
Actb L/L
Actb L/L Cre
D.
Relative Expression
0
1
2
3
4
βcyto-actin
γcyto-actin
αsm-actin
Total actin

Figure 3.3: β_{cyto}-Actin and γ_{cyto}-actin colocalize in MEFs. A-D: Cells were sparsely plated on fibronectin, incubated for 3 hours, and subsequently co-stained with antibodies to β_{cyto}-actin (green) and γ_{cyto}-actin (red). *Actg1*$^{-/-}$ (A) and *Actb*$^{L/L}$ *Cre* (B) cells demonstrate the isoform specificity of γ_{cyto}-actin and β_{cyto}-actin antibodies respectively. In wild-type cells (C), all actin structures were co-labeled with β_{cyto}- and γ_{cyto}-actin antibodies. High magnification of membrane protrusions (D) demonstrates colocalization of β_{cyto}- and γ_{cyto}-actin in lamellipodia. Cells were maintained in 10% serum. Scale bars: 20 μm.

Figure 3.3

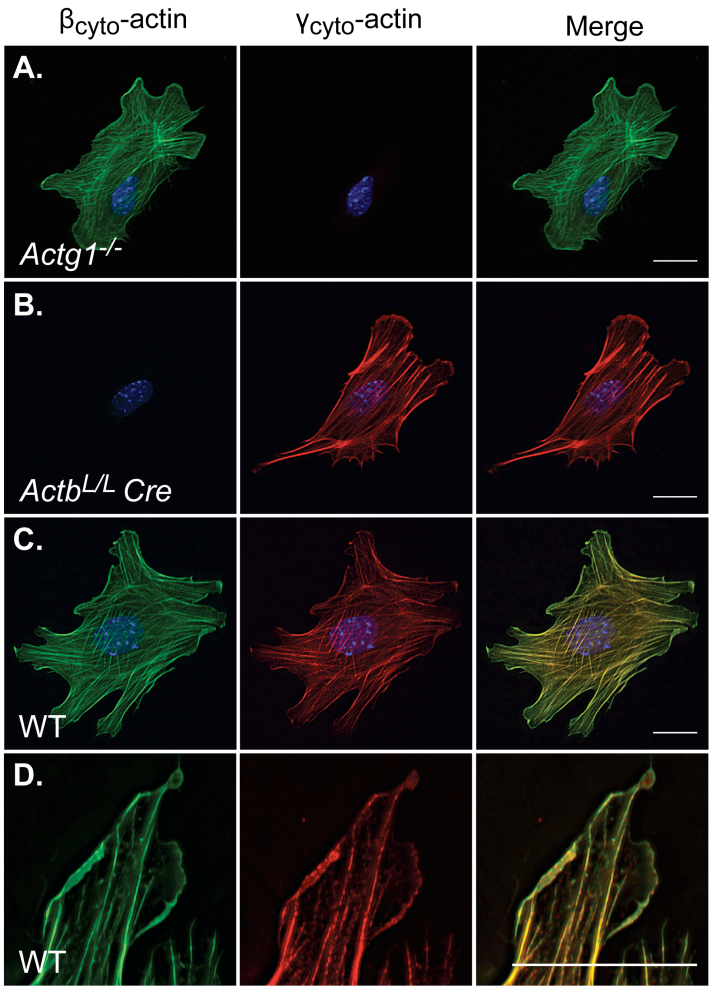

Figure 3.4: Severe growth deficiency in the absence of β_{cyto}-actin. **A:** Pan-actin labeled immunoblot of supernatant (S) and pellet (P) fractions from cell lysates after high-speed centrifugation. G-actin and F-actin pools are found in the supernatant and pellet fractions respectively. **B:** Quantitative Western blot results of G- to F-actin ratios (n = 3). **C:** Growth curves of *Actb*$^{L/L}$ and *Actb*$^{L/L}$ *Cre* MEFs (n = 4). Cell numbers were significantly decreased in *Actb*$^{L/L}$ *Cre* MEFs from day 2 onward as determined by an unpaired t test at each time-point. **D:** Mean percentage of apoptotic cells, defined as FITC-positive and PI-negative (n = 4). **E:** Dot plots from FITC-Annexin V flow cytometric analyses. The lower-right box represents early apoptotic cells while the upper right box represents dead cells. **F:** Mean percentage of cells containing multiple nuclei from at least 3-4 independent experiments. More than 250 cells were counted per experiment. **G:** Representative traces from flow cytometric analyses of DNA content by propidium iodide staining. Asterisks denote significant differences ($p < 0.05$); error bars represent s.e.m.

Figure 3.4

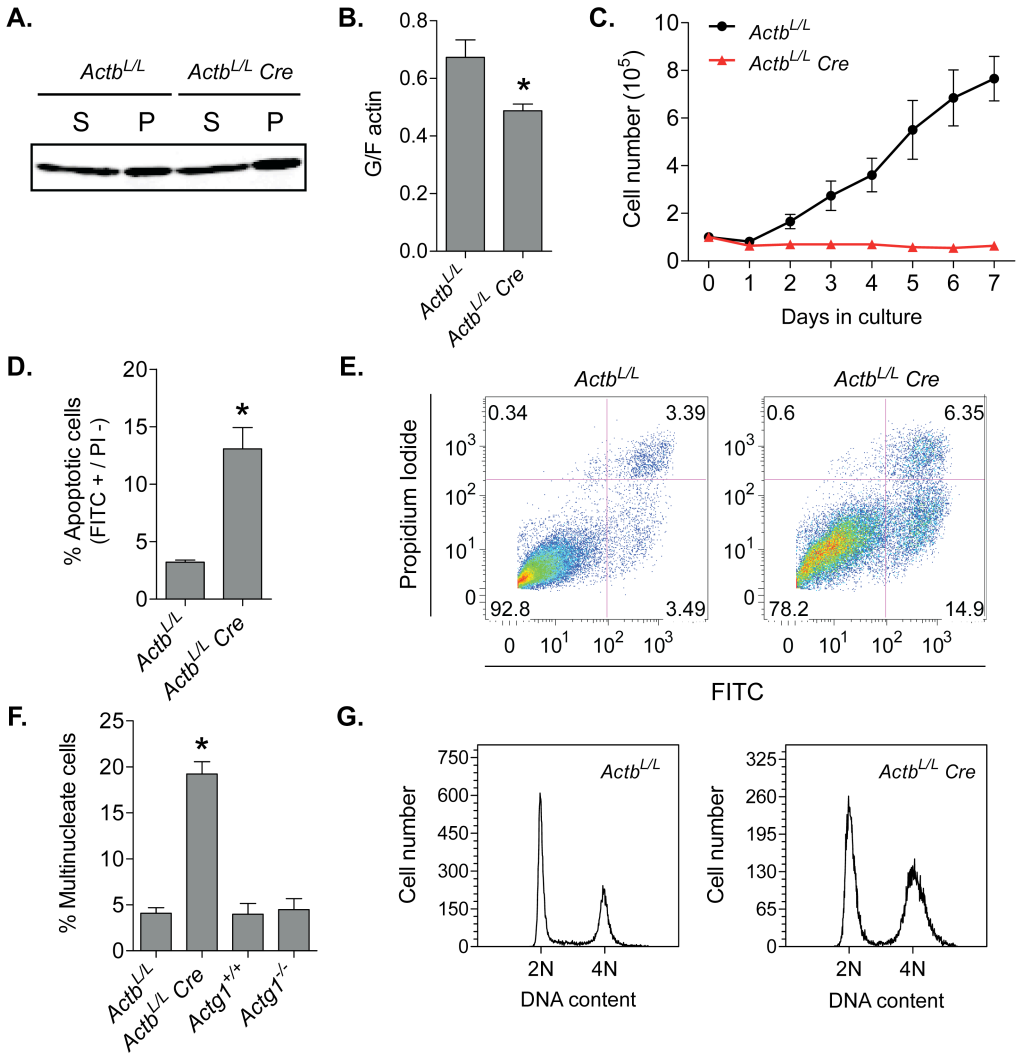
A.
Actb L/L
Actb L/L Cre
S
P
S
P
B.
G/F actin
0.8
0.6
0.4
0.2
0.0
*
Actb L/L
Actb L/L Cre
C.
Actb L/L
Actb L/L Cre
Cell number (10 5)
10
8
6
4
2
0
0 1 2 3 4 5 6 7
Days in culture
D.
% Apoptotic cells (FITC + / PI -)
20
15
10
5
0
*
Actb L/L
Actb L/L Cre
E.
Actb L/L
Actb L/L Cre
Propidium Iodide
0.34
3.39
92.8
3.49
0.6
6.35
78.2
14.9
0 10 1 10 2 10 3
FITC
F.
% Multinucleate cells
25
20
15
10
5
0
*
Actb L/L
Actb L/L Cre
Actg1 +/+
Actg1 -/-
G.
Actb L/L
Actb L/L Cre
Cell number
750
600
450
300
150
0
325
260
195
130
65
0
2N
4N
DNA content

Figure 3.5: Impaired migration in β_{cyto}-actin knockout MEFs. A: Randomly migrating cells were tracked at 10-minute intervals for 4 hours. Shown are representative examples of individual migration tracks of *Actb*$^{L/L}$ and *Actb*$^{L/L}$ *Cre* MEFs combined into a single figure. **B:** Quantification of migration velocity ($n \geq 88$ cells per genotype). **C:** Directionality of cell migration was calculated as the linear distance (D) over the total track distance (T) of a cell. **D-E:** Individual frames (D) and kymographs (E) from DIC time-lapse movies of *Actb*$^{L/L}$ and *Actb*$^{L/L}$ *Cre* MEFs. Kymographs show lamellipodial activity along the lines in respective DIC images. Images in panel D represent the last frame of the 10-minute movie. Line: 10 μm. **F-G:** Quantification of kymographs showing the frequency, persistence, and velocity of protrusion (F) and retraction (G) events. For all box and whisker plots, whiskers indicate maximum and minimum values, the box represents the 25th-75th quartile, and the line indicates the median. Asterisks denote significant differences ($p < 0.05$) from each of the other genotypes.

Figure 3.5

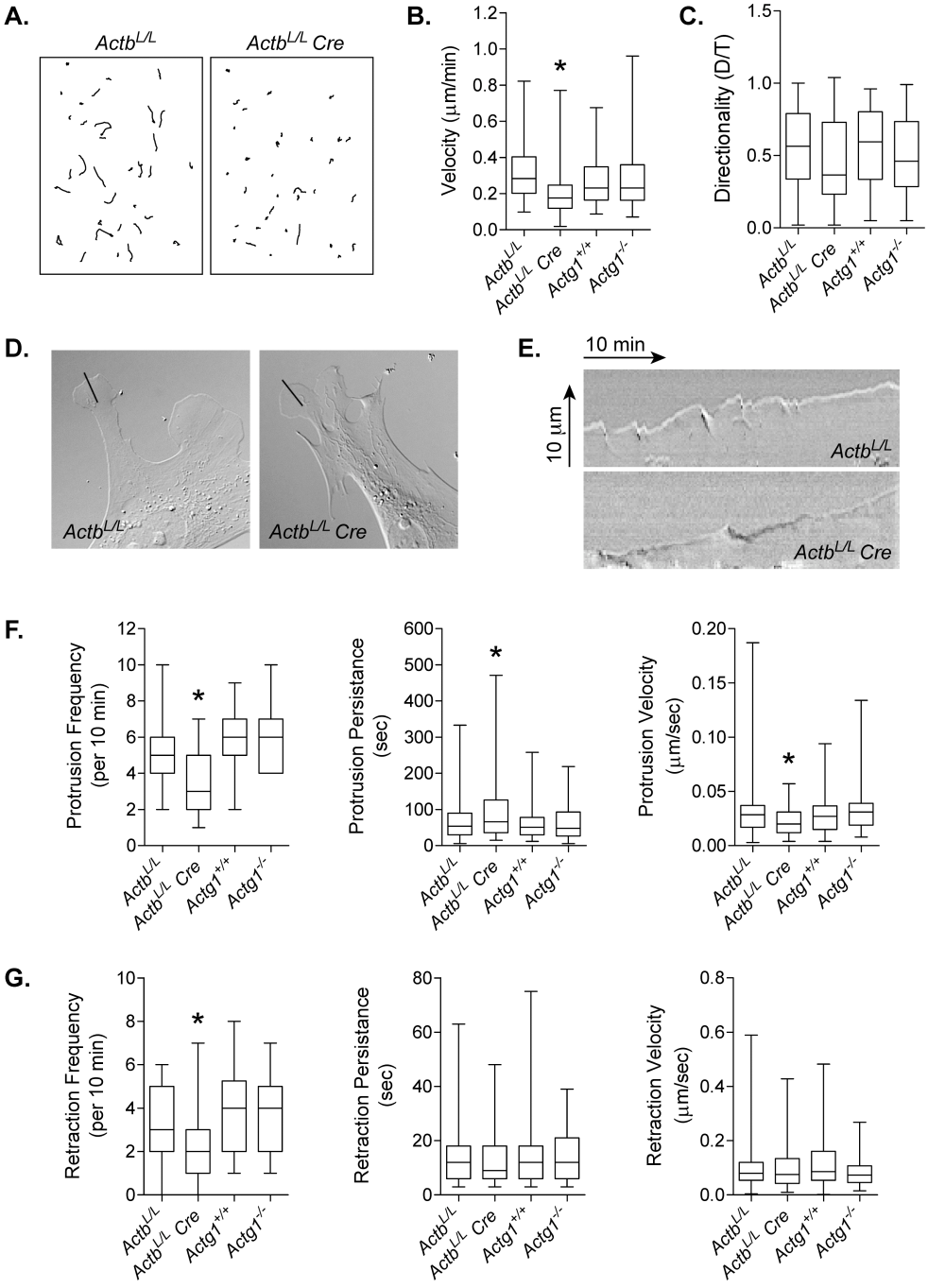
A.
Actb L/L
Actb L/L Cre
B.
Velocity (µm/min)
1.2
1.0
0.8
0.6
0.4
0.2
0.0
*
Actb L/L
Actb L/L Cre
Actg1 +/+
Actg1 -/-
C.
Directionality (D/T)
1.5
1.0
0.5
0.0
Actb L/L
Actb L/L Cre
Actg1 +/+
Actg1 -/-
D.
Actb L/L
Actb L/L Cre
E.
10 min
10 µm
Actb L/L
Actb L/L Cre
F.
Protrusion Frequency (per 10 min)
12
10
8
6
4
2
0
*
Actb L/L
Actb L/L Cre
Actg1 +/+
Actg1 -/-
Protrusion Persistance (sec)
600
500
400
300
200
100
0
*
Actb L/L
Actb L/L Cre
Actg1 +/+
Actg1 -/-
Protrusion Velocity (µm/sec)
0.20
0.15
0.10
0.05
0.00
*
Actb L/L
Actb L/L Cre
Actg1 +/+
Actg1 -/-
G.
Retraction Frequency (per 10 min)
10
8
6
4
2
0
*
Actb L/L
Actb L/L Cre
Actg1 +/+
Actg1 -/-
Retraction Persistance (sec)
80
60
40
20
0
Actb L/L
Actb L/L Cre
Actg1 +/+
Actg1 -/-
Retraction Velocity (µm/sec)
0.8
0.6
0.4
0.2
0.0
Actb L/L
Actb L/L Cre
Actg1 +/+
Actg1 -/-

Discussion

Actb$^{-/-}$ mice were early embryonic lethal, indicating β_{cyto}-actin is an essential gene. Our data is consistent with the previously reported embryonic lethality of mice homozygous for hypomorphic alleles of *Actb* (42, 43). We observed less than expected frequencies of *Actb*$^{-/-}$ mice as early as E7.5, with those recovered at this stage appearing to have already begun degenerating. Therefore, the lethality of *Actb*$^{-/-}$ mice begins prior to E7.5. In contrast, *Actg1*$^{-/-}$ mice are fully viable throughout development, with some lethality occurring post-birth (45, 62). Taken together, we conclude that β_{cyto}-actin, but not γ_{cyto}-actin, is an essential gene required for early embryogenesis. Rapid cell growth and dynamic cell movements are critical processes during early stages of embryonic development, both of which were shown to be severely impaired in *Actb*$^{L/L}$ *Cre* MEFs. Therefore, we speculate that the lethality of *Actb*$^{-/-}$ mice is due largely to impaired cell growth and migration.

Using an *in vitro* random cell migration assay, we showed that β_{cyto}-actin knockout leads to dramatic migration defects, whereas cell motility in *Actg1*$^{-/-}$ cells was normal. One possible explanation for this unique requirement of β_{cyto}-actin during cell migration is differential sub-cellular localization of β_{cyto}- and γ_{cyto}-actin. Several studies have reported preferential localization of β_{cyto}-actin at the leading edge in migrating cells (24-27, 56). Furthermore, zipcode-binding protein 1 (ZBP1) has been shown to regulate the asymmetric targeting of β_{cyto}-actin mRNA to lamellipodia (28, 32, 69). Under our cell culture conditions, however, we did not observe differential localization patterns of β_{cyto}- and γ_{cyto}-actin using verified actin-isoform specific antibodies. One reason for the

discrepancy between our results and those reported previously is that we used dye-conjugated primary antibodies, which were shown by our lab to give different results compared to primary-secondary antibody combinations (63). Nonetheless, our observations that β_{cyto}- and γ_{cyto}-actin both localize to the leading edge in wild-type cells, suggests that the migration defect in *Actb*$^{L/L}$ *Cre* cells is not due to localization differences between β_{cyto}- and γ_{cyto}-actin.

Alternatively, the presence of arginylated β_{cyto}-actin but not γ_{cyto}-actin *in vivo* (39) may confer a specific function for β_{cyto}-actin in cell migration. Evidence from one study suggests that arginylation of β_{cyto}-actin helps to regulate lamella formation and motility in fibroblasts (38). It has therefore been suggested that arginylation of β_{cyto}-actin results in the formation of filaments evenly coated with bulky positive charges, which prevents close interaction of filaments and thus facilitates the formation of the loose dendritic actin network found in lamellapodia (38, 65). Whether the motility defects observed in *Actb*$^{L/L}$ *Cre* cells is specifically due to the loss of arginylated actin will require further investigation.

Inherent biochemical differences between β_{cyto}- and γ_{cyto}-actin provide an additional explanation for the differential requirement of the two isoforms during cell migration. Using a baculovirus-driven expression system to produce pure populations of β_{cyto}- and γ_{cyto}-actin, Bergeron et al. (61) recently demonstrated distinct biochemical properties of the two isoforms. β_{cyto}-Actin was shown to polymerize and depolymerize more rapidly than γ_{cyto}-actin, indicating β_{cyto}-actin as the more dynamic isoform (61). This report is consistent with our observations of reduced leading edge dynamics in β_{cyto}-

actin knockout cells but not *Actg1*$^{-/-}$ cells. In addition to fewer protrusion and retraction events, we observed a significant decrease in protrusion velocity, indicative of a slower rate of actin polymerization. Our colocalization observations demonstrate that both β_{cyto}-actin and γ_{cyto}-actin are found at the leading edge. In fact, β_{cyto}- and γ_{cyto}-actin appear to readily copolymerize *in vitro* (61), suggesting that our observations of colocalization reflect copolymers of actin isoforms. Bergeron et al. (61) show that the biochemical behavior of β_{cyto}- and γ_{cyto}-actin copolymers reflects the relative percentage of each isoform. Therefore, actin filament properties can be modulated by the ratio of β_{cyto}-actin to γ_{cyto}-actin. Taken together, our results indicate that actin filaments at the leading edge require incorporation of β_{cyto}-actin for proper membrane protrusion dynamics during cell migration.

In addition to reduced membrane dynamics, the observed increase in stress fibers likely also contributed to impaired migration in *Actb*$^{L/L}$ *Cre* MEFs. In contrast with *Actg1*$^{-/-}$ cells, which showed no change in the G- to F-actin ratio (62), F-actin content was increased in β_{cyto}-actin knockout cells. Given that γ_{cyto}-actin was upregulated in *Actb*$^{L/L}$ *Cre* cells, increased F-actin content is consistent with the report that γ_{cyto}-actin polymerizes slower and exhibits greater filament stability than β_{cyto}-actin (61). We also observed upregulation of α_{sm}-actin in *Actb*$^{L/L}$ *Cre* cells, which has been shown to correlate with more prominent stress fibers and decreased cell motility (70).

We previously demonstrated that ablation of γ_{cyto}-actin leads to a mild growth impairment resulting from reduced cell survival (62). In contrast, β_{cyto}-actin knockout MEFs were severely growth impaired and exhibited a significant increase in apoptosis.

Thus, while γ_{cyto}-actin confers advantages for cell growth and survival, β_{cyto}-actin is absolutely essential for maintaining cell growth potential. Whether increased apoptosis in *Actb*$^{L/L}$ *Cre* MEFs is due to a direct function for β_{cyto}-actin in cell survival is unknown. Increased apoptosis, however, most likely cannot fully account for the zero growth rate of *Actb*$^{L/L}$ *Cre* MEFs, suggesting that proliferation may also be affected by the loss of β_{cyto}-actin. In addition, we observed an increase in the percent of multinucleated cells in *Actb*$^{L/L}$ *Cre* MEFs but not in *Actg1*$^{-/-}$ MEFs, indicating a possible unique function for β_{cyto}-actin during cytokinesis. In fact, it was recently reported that β_{cyto}-actin is enriched at the contractile ring during cell division (35). Since β_{cyto}-actin is the more dynamic isoform (61), we postulate that it is important for the rapid reorganization of the actin cytoskeleton during cytokinesis.

Given the lethality of *Actb*$^{-/-}$ mice, it is not surprising that β_{cyto}-actin homozygous mutations have never been identified in humans. However, there are two independent reports of β_{cyto}-actin heterozygous mutations (71, 72). In one case the mutation was identified in identical twins and associated with multiple developmental abnormalities (72, 73). In the second case the mutation was associated with recurrent infection resulting from neutrophil dysfunction, including depressed chemotactic responses (71). In addition, significant increases in β_{cyto}-actin expression levels have been observed in highly invasive variants of several different tumor cell lines (74-76), suggesting a potential role for β_{cyto}-actin in tumor metastasis. These reports are in agreement with our evidence that β_{cyto}-actin is essential for embryogenesis and plays a critical role during cell migration. Generation of β_{cyto}-actin conditional knockouts will be necessary to further

study the *in vivo* requirement of β_{cyto}-actin during specific developmental processes and in different migratory cell types.

Chapter 4

Conclusions and Future Directions

Actin is fundamental to eukaryotic life. In mammals there exists six different actin isoforms, of which only β_{cyto}- and γ_{cyto}-actin are ubiquitously expressed. The fact that β_{cyto}- and γ_{cyto}-actin, which are 99% identical, have been exactly conserved from birds to mammals has led to the hypothesis that the two isoforms have unique functions. Since actin is essential for embryonic development, it was therefore predicted that β_{cyto}- or γ_{cyto}-actin null mice would be embryonic lethal. As described in Chapter 2, embryogenesis in γ_{cyto}-actin null mice was surprisingly normal, indicating that β_{cyto}-actin can largely compensate for the loss of γ_{cyto}-actin during embryonic development. Nonetheless, γ_{cyto}-actin null embryos exhibited mild developmental delays and decreased postnatal survival. Furthermore, γ_{cyto}-actin null primary MEFs had a mild growth deficiency and a slight increase in apoptosis, despite total actin levels being maintained. These data suggest that while γ_{cyto}-actin is largely dispensable for embryonic development, it does confer growth and survival advantages. As described in Chapter 3 and in contrast to γ_{cyto}-actin null mice, β_{cyto}-actin null mice were early embryonic lethal. Together, these data indicate that β_{cyto}-actin but not γ_{cyto}-actin is an essential gene required for early embryonic development.

Given the very early lethality of β_{cyto}-actin null embryos, it was difficult to assess how β_{cyto}-actin might be important in development. Therefore, we established a system for knocking out β_{cyto}-actin in primary MEFs in order to assess the functional specificity of β_{cyto}-actin in cellular processes important for development. One key feature of early embryonic development is rapid cell growth and proliferation. β_{cyto}-Actin knockout

MEFs were severely growth impaired, showing no increase in cell number over a 7-day period. Furthermore, β_{cyto}-actin knockout cells exhibited a significant increase in apoptosis and in the percentage of multinucleate cells. From these data, we postulate that growth deficiencies in the absence of β_{cyto}-actin contribute to the early embryonic lethality of β_{cyto}-actin null mice.

Perhaps the most well recognized role for actin during development is in morphogenesis, where it provides the necessary forces for cell movements. Therefore, we investigated the ability of β_{cyto}- and γ_{cyto}-actin knockout cells to migrate. Not surprisingly given the normal development of γ_{cyto}-actin null mice, we did not observe any migratory defects in γ_{cyto}-actin null MEFs. In contrast, migration was severely impaired in β_{cyto}-actin knockout MEFs, suggesting that migration defects also contributed to the embryonic lethality of β_{cyto}-actin null mice. To determine whether β_{cyto}-actin is required for cell migration *in vivo*, a conditional knockout approach using our β_{cyto}-actin floxed allele will be necessary. Given the relatively long half-life of actin, it will be difficult to assess migration events during development using conditional knockouts. However, cell migration is also essential in adult organisms, particularly in cells of the immune system; therefore, we are interested in crossing β_{cyto}-actin floxed mice to CD4-Cre animals (77) in order to assess whether β_{cyto}-actin is required for T-cell migration *in vivo*.

The distinct phenotypes of β_{cyto}- and γ_{cyto}-actin knockout animals and cells presented here and in previous work from the Ervasti laboratory (44, 45, 63) provide considerable evidence that the two cytoplasmic actins have unique biological roles. Nevertheless, the

molecular mechanism(s) of isoform-specific functions remains elusive. Using evidence from the literature, we provide here several ideas to explain how β_{cyto}- and γ_{cyto}-actin are functionally distinct.

It was recently demonstrated that the four amino acid differences between β_{cyto}- and γ_{cyto}-actin confer distinct biochemical properties between the two isoforms (61). Using purified β_{cyto}- and γ_{cyto}-actin produced in a recombinant baculovirus system, Bergeron et al. (61) provide convincing evidence that β_{cyto}-actin is the more dynamic of the two isoforms. Specifically, β_{cyto}-actin exhibited a faster monomeric nucleotide exchange rate, a shorter nucleation phase, a faster elongation rate, and depolymerized more rapidly than γ_{cyto}-actin. These data are in line with several of the phenotypes we reported for β_{cyto}-actin knockout cells. Using kymograph analyses, we observed reduced protrusion and retraction frequencies as well as reduced protrusion velocity at the leading edge in β_{cyto}-actin knockout cells. Cell motility is driven by rapid polymerization and depolymerization of branched actin filaments at the leading edge (6), therefore our observations of reduced leading edge dynamics and cell motility in β_{cyto}-actin knockout cells is consistent with β_{cyto}-actin being the more dynamic isoform. Conversely, γ_{cyto}-actin is slower to polymerize and exhibits greater filament stability than β_{cyto}-actin (61). In β_{cyto}-actin knockout cells, we observed elevated levels of γ_{cyto}-actin along with increased F-actin content, which is fitting with the idea that γ_{cyto}-actin is less dynamic than β_{cyto}-actin.

Migration occurs as a result of a coordinated balance between the mechanical forces generated by actin polymerization at the leading edge and the resisting forces

generated by cell adhesions. Actin polymerization and filament organization is tightly linked to focal adhesion formation and disassembly, therefore altered actin dynamics in β_{cyto}-actin knockout cells could also cause changes in focal adhesion content and thus further contribute to the cell motility defect. Whether focal adhesion content is altered in β_{cyto}-actin knockout cells would be an interesting line of future investigation.

In addition to cell migration, the process of cell division and cytokinesis requires a dynamic actin cytoskeleton. During cell division, the actin cytoskeleton rapidly reorganizes such that the cell becomes rounded and a contractile ring composed of actin and myosin filaments forms at the cell cortex. As the contractile ring constricts, the actin filaments must depolymerize in proportion to the ring's circumference. The requirement for a dynamic cytoskeleton during cytokinesis suggests that β_{cyto}-actin may also be important for this process. Indeed, we observed a significant increase in multinucleate cells in β_{cyto}-actin knockout MEFs but not γ_{cyto}-actin null MEFs. Our attempts to synchronize primary MEFs by serum starvation in order to more rigorously characterize this phenotype were unsuccessful. Therefore, drug-induced synchronization of primary MEFs may be necessary to fully characterize the cytokinesis defect in β_{cyto}-actin knockout cells. We predict that cytokinesis proceeds more slowly in the absence of the more dynamic β_{cyto}-actin isoform, resulting in some cells fusing together before cytokinesis can be completed.

The four amino acids that vary between β_{cyto}- and γ_{cyto}-actin reside in the N-terminus. A recent structural analysis of F-actin demonstrates that this part of the protein extends out from the filament where it is readily accessible to actin binding

proteins (ABPs) (78). These data suggest that the divergent amino acids between the two isoforms could readily influence interactions with certain ABPs. Identification of such proteins has been challenging due to the ubiquitous expression of β_{cyto}- and γ_{cyto}-actin and the difficulty in obtaining pure populations of each. Tzima et al. provide data that suggests annexin V binds specifically to γ_{cyto}-actin at the plasma membrane of platelets; however, their use of unverified actin-isoform specific antibodies raises some doubts about their results (60). Differential binding affinities have been observed between muscle and cytoplasmic actins. Specifically, several ABPs have been shown to interact more strongly with cytoplasmic actins than with α_{sk}-actin, including profilin (79, 80), thymosin β4 (81), L-plastin (82), βcap73 (59), and Ezrin (83). Furthermore, cofilin binds with greater cooperativity to cytoplasmic actin filaments than α_{sk}-actin filaments (84). Whether β_{cyto}- and γ_{cyto}-actin differentially interact with certain ABPs remains an open question. With the recent establishment of a baculovirus-driven expression system for the two cytoplasmic actin isoforms (61), it will now be possible to biochemically analyze the interactions between each actin isoform and various ABPs. As an alternative approach, affinity purification of actin and associated proteins from both β_{cyto}- and γ_{cyto}-actin knockout cell lysates followed by 2D gel electrophoresis and mass spectrometry may help to identify unique binding partners for each isoform.

To test whether it is in fact the amino acid differences and not differences in coding or untranslated sequences that confer functional specificity, one could carry out a rescue experiment using "converted" actin constructs. In such converted constructs, the nucleotide sequences encoding the 4 amino acids that are different between the isoforms

would be converted to those of the alternate isoform, leaving the remaining coding sequence and untranslated regions the same. As such, a 'β_{cyto}-actin converted γ_{cyto}-actin' construct would produce γ_{cyto}-actin protein from a construct containing mostly β_{cyto}-actin coding sequences and the β_{cyto}-actin untranslated regions (and vice versa). If the amino acid differences between β_{cyto}- and γ_{cyto}-actin do indeed confer functional specificity for β_{cyto}-actin in cell migration then the 'β_{cyto}-actin converted γ_{cyto}-actin' construct will not be able to rescue the phenotype while a 'γ_{cyto}-actin converted β_{cyto}-actin' construct will. If the result is reversed or only a partial rescue is observed that would indicate that coding sequence differences or the untranslated regions confer functional specificity. In fact, there was a recent *in vitro* study suggesting that the differences in coding sequence between β_{cyto}- and γ_{cyto}-actin confer different translation rates. γ_{cyto}-Actin was translated more slowly than β_{cyto}-actin, resulting in the exposure of a normally hidden lysine residue near the N-terminus, which in turn attracts the ubiquitin conjugation machinery upon cotranslational arginylation of γ_{cyto}-actin at the N-terminus. Such ubiquitination leads to the preferential degradation of arginylated γ_{cyto}-actin (39).

Additionally, a regulatory element in the untranslated region of β_{cyto}-actin mRNA has also been suggested to confer functional specificity. The 3'-untranslated region (UTR) of β_{cyto}-actin mRNA contains a 54 nucleotide zipcode sequence not found in γ_{cyto}-actin mRNA. The zipcode sequence is recognized and bound by the zipcode binding protein 1 (ZBP1), which mediates the asymmetric localization of β_{cyto}-actin to the leading edge and is thought to be important for cell motility (reviewed in (64)). Using a rescue strategy, our β_{cyto}-actin knockout cells provide an excellent model system for specifically

testing the importance of the β_{cyto}-actin zipcode sequence in cell migration. If the zipcode sequence is indeed important for cell motility, then a β_{cyto}-actin construct lacking the zipcode sequence should be unable to rescue the migration phenotype to the same extent as a wild-type construct. As an additional approach, the 3'-UTR of β_{cyto}-actin could be replaced with the 3'-UTR of γ_{cyto}-actin, which does not contain the zipcode sequence. Conversely, the 3'-UTR of γ_{cyto}-actin could be swapped for the 3'-UTR of β_{cyto}-actin in order to assess whether γ_{cyto}-actin under the regulation of the β_{cyto}-actin 3'-UTR is sufficient to rescue the migration phenotype. We predict that this will not be the case given the biochemical differences between the two isoforms, however, a partial rescue may be observed.

It is also possible that gene expression of ABPs is dysregulated in β_{cyto}-actin knockout cells, thus disrupting the normal function of actin and contributing to the observed phenotypes. In support of this idea are several bodies of work that implicate a role for actin in gene transcription (reviewed in (9)). First, actin has been found in association with chromatin-remodeling and histone acetyl transferase complexes, suggesting a functional link between actin and regulation of chromatin structure. Second, actin is required for transcription by all three nuclear RNA polymerases, where it appears to play a role in multiple stages of the transcription process. There is some evidence, albeit weak, that the actin isoform associated with chromatin remodeling complexes and RNA polymerases is β_{cyto}-actin (85-88). Finally, the serum response factor (SRF) gene regulatory pathway is tightly regulated by actin dynamics. Monomeric actin binds to myocardin-related transcription factors (MRTFs) and inhibits their ability to bind and

activate the transcription factor SRF. Importantly, MRTFs trigger the expression of a subset of SRF target genes that are primarily actin regulators, thus creating an autoregulatory feedback circuit. In β_{cyto}-actin knockout cells we observed a decrease in the G- to F-actin ratio, indicating that the levels of G-actin are decreased. As such, one would predict an upregulation of MRTF-SRF target genes. All together, there is sufficient precedent for investigating perturbations in gene expression in β_{cyto}-actin knockout cells. To this end, we are interested in utilizing a Cytoskeleton Regulators RT^2 PCR Array (SA Biosciences) to compare the expression of a focused panel of genes between wild-type and β_{cyto}-actin knockout MEFs.

Total actin expression levels were maintained in β_{cyto}-actin knockout cells as a result of an upregulation of other actin isoforms. While the most closely related γ_{cyto}-actin isoform was predictably upregulated, α_{smooth}-actin expression was surprisingly increased as well. This raises the possibility that elevated expression of α_{smooth}-actin contributes to the observed phenotypes in β_{cyto}-actin knockout cells. Indeed, α_{smooth}-actin expression has been shown to correlate with more prominent stress fibers and decreased cell motility (70). Furthermore, α_{smooth}-actin is the most significant marker of myofibroblasts, a cell-type with a phenotype intermediate between fibroblasts and smooth muscle cells (89). Hallmarks of the myofibroblast are the formation of contractile bundles composed of actin and myosin and well-developed cell-matrix interactions. It is therefore plausible that the elevated expression of α_{smooth}-actin in β_{cyto}-actin knockout cells leads to a myofibroblast-like phenotype. In order to test the extent to which α_{smooth}-actin is contributing to the phenotypes in β_{cyto}-actin knockout cells, we are

interested in knocking down α_{smooth}-actin expression by siRNA and testing for phenotypic rescue. Presumably, total actin levels will continue to be maintained as a result of a further increase in γ_{cyto}-actin protein expression, however, if this is not the case the results from such an experiment will be difficult to interpret.

The distinct phenotypes observed in β_{cyto}- and γ_{cyto}-actin knockout mice and cells demonstrate that while β_{cyto}- and γ_{cyto}-actin can compensate for each other to a limited extent, they also have unique biological functions. The use of *in vivo*, tissue-specific ablation studies will most definitively reveal these distinct biological roles. To this end, the Ervasti laboratory is currently investigating the role of β_{cyto}- and γ_{cyto}-actin in the auditory and nervous system using tissue-specific knockouts. Furthermore, we are working in collaboration with Dr. Yoji Shimizu to examine whether β_{cyto}-actin is necessary for *in vivo* T-cell migration and function. In parallel with these *in vivo* studies, the *in vitro* knockout culture strategy established through my thesis work provides an excellent model system for dissecting apart the molecular mechanism(s) that confer functional specificity between β_{cyto}- and γ_{cyto}-actin.

References

1. De La Cruz, E. M., Mandinova, A., Steinmetz, M. O., Stoffler, D., Aebi, U., and Pollard, T. D. (2000) Polymerization and structure of nucleotide-free actin filaments. *J Mol Biol* 295, 517-526

2. Pollard, T. D. (1986) Assembly and dynamics of the actin filament system in nonmuscle cells. *J Cell Biochem* 31, 87-95

3. Pollard, T. D., Blanchoin, L., and Mullins, R. D. (2000) Molecular mechanisms controlling actin filament dynamics in nonmuscle cells. *Annu Rev Biophys Biomol Struct* 29, 545-576

4. Chhabra, E. S., and Higgs, H. N. (2007) The many faces of actin: matching assembly factors with cellular structures. *Nat Cell Biol* 9, 1110-1121

5. Winder, S. J., and Ayscough, K. R. (2005) Actin-binding proteins. *J Cell Sci* 118, 651-654

6. Pollard, T. D., and Borisy, G. G. (2003) Cellular motility driven by assembly and disassembly of actin filaments. *Cell* 112, 453-465

7. Pollard, T. D., and Cooper, J. A. (2009) Actin, a central player in cell shape and movement. *Science* 326, 1208-1212

8. Posern, G., and Treisman, R. (2006) Actin' together: serum response factor, its cofactors and the link to signal transduction. *Trends Cell Biol* 16, 588-596

9. Zheng, B., Han, M., Bernier, M., and Wen, J. K. (2009) Nuclear actin and actin-binding proteins in the regulation of transcription and gene expression. *FEBS J* 276, 2669-2685

10. Pollard, T. D. (2010) Mechanics of cytokinesis in eukaryotes. *Curr Opin Cell Biol* 22, 50-56

11. Marston, D. J., and Goldstein, B. (2006) Actin-based forces driving embryonic morphogenesis in Caenorhabditis elegans. *Curr Opin Genet Dev* 16, 392-398

12. Vandekerckhove, J., and Weber, K. (1978) At least six different actins are expressed in a higher mammal: an analysis based on the amino acid sequence of the amino-terminal tryptic peptide. *J Mol Biol* 126, 783-802

13. Rubenstein, P. A. (1990) The functional importance of multiple actin isoforms. *Bioessays* 12, 309-315

14. Kumar, A., Crawford, K., Close, L., Madison, M., Lorenz, J., Doetschman, T., Pawlowski, S., Duffy, J., Neumann, J., Robbins, J., Boivin, G. P., O'Toole, B. A., and Lessard, J. L. (1997) Rescue of cardiac alpha-actin-deficient mice by enteric smooth muscle gamma-actin. *Proc Natl Acad Sci U S A* 94, 4406-4411

15. Schildmeyer, L. A., Braun, R., Taffet, G., Debiasi, M., Burns, A. E., Bradley, A., and Schwartz, R. J. (2000) Impaired vascular contractility and blood pressure homeostasis in the smooth muscle alpha-actin null mouse. *FASEB J* 14, 2213-2220

16. Crawford, K., Flick, R., Close, L., Shelly, D., Paul, R., Bove, K., Kumar, A., and Lessard, J. (2002) Mice lacking skeletal muscle actin show reduced muscle strength and growth deficits and die during the neonatal period. *Mol Cell Biol* 22, 5887-5896

17. Jaeger, M. A., Sonnemann, K. J., Fitzsimons, D. P., Prins, K. W., and Ervasti, J. M. (2009) Context-dependent functional substitution of alpha-skeletal actin by gamma-cytoplasmic actin. *FASEB J* 23, 2205-2214

18. Otey, C. A., Kalnoski, M. H., and Bulinski, J. C. (1987) Identification and quantification of actin isoforms in vertebrate cells and tissues. *J Cell Biochem* 34, 113-124

19. Erba, H. P., Eddy, R., Shows, T., Kedes, L., and Gunning, P. (1988) Structure, chromosome location, and expression of the human gamma-actin gene: differential evolution, location, and expression of the cytoskeletal beta- and gamma-actin genes. *Mol Cell Biol* 8, 1775-1789

20. McHugh, K. M., Crawford, K., and Lessard, J. L. (1991) A comprehensive analysis of the developmental and tissue-specific expression of the isoactin multigene family in the rat. *Dev Biol* 148, 442-458

21. Khaitlina, S. Y. (2001) Functional specificity of actin isoforms. *Int Rev Cytol* 202, 35-98

22. Leavitt, J., Ng, S. Y., Aebi, U., Varma, M., Latter, G., Burbeck, S., Kedes, L., and Gunning, P. (1987) Expression of transfected mutant beta-actin genes: alterations of cell morphology and evidence for autoregulation in actin pools. *Mol Cell Biol* 7, 2457-2466

23. Ng, S. Y., Erba, H., Latter, G., Kedes, L., and Leavitt, J. (1988) Modulation of microfilament protein composition by transfected cytoskeletal actin genes. *Mol Cell Biol* 8, 1790-1794

24. Hoock, T. C., Newcomb, P. M., and Herman, I. M. (1991) Beta actin and its mRNA are localized at the plasma membrane and the regions of moving cytoplasm during the cellular response to injury. *J Cell Biol* 112, 653-664

25. Hill, M. A., and Gunning, P. (1993) Beta and gamma actin mRNAs are differentially located within myoblasts. *J Cell Biol* 122, 825-832

26. Bassell, G. J., Zhang, H., Byrd, A. L., Femino, A. M., Singer, R. H., Taneja, K. L., Lifshitz, L. M., Herman, I. M., and Kosik, K. S. (1998) Sorting of beta-actin mRNA and protein to neurites and growth cones in culture. *J Neurosci* 18, 251-265

27. Micheva, K. D., Vallee, A., Beaulieu, C., Herman, I. M., and Leclerc, N. (1998) beta-Actin is confined to structures having high capacity of remodelling in developing and adult rat cerebellum. *Eur J Neurosci* 10, 3785-3798

28. Kislauskis, E. H., Zhu, X., and Singer, R. H. (1994) Sequences responsible for intracellular localization of beta-actin messenger RNA also affect cell phenotype. *J Cell Biol* 127, 441-451

29. Ross, A. F., Oleynikov, Y., Kislauskis, E. H., Taneja, K. L., and Singer, R. H. (1997) Characterization of a beta-actin mRNA zipcode-binding protein. *Mol Cell Biol* 17, 2158-2165

30. Oleynikov, Y., and Singer, R. H. (2003) Real-time visualization of ZBP1 association with beta-actin mRNA during transcription and localization. *Curr Biol* 13, 199-207

31. Huttelmaier, S., Zenklusen, D., Lederer, M., Dictenberg, J., Lorenz, M., Meng, X., Bassell, G. J., Condeelis, J., and Singer, R. H. (2005) Spatial regulation of beta-actin translation by Src-dependent phosphorylation of ZBP1. *Nature* 438, 512-515

32. Kislauskis, E. H., Zhu, X., and Singer, R. H. (1997) beta-Actin messenger RNA localization and protein synthesis augment cell motility. *J Cell Biol* 136, 1263-1270

33. Yao, J., Sasaki, Y., Wen, Z., Bassell, G. J., and Zheng, J. Q. (2006) An essential role for beta-actin mRNA localization and translation in Ca2+-dependent growth cone guidance. *Nat Neurosci* 9, 1265-1273

34. Jonson, L., Vikesaa, J., Krogh, A., Nielsen, L. K., Hansen, T., Borup, R., Johnsen, A. H., Christiansen, J., and Nielsen, F. C. (2007) Molecular composition of IMP1 ribonucleoprotein granules. *Mol Cell Proteomics* 6, 798-811

35. Dugina, V., Zwaenepoel, I., Gabbiani, G., Clement, S., and Chaponnier, C. (2009) Beta and gamma-cytoplasmic actins display distinct distribution and functional diversity. *J Cell Sci* 122, 2980-2988

36. Perrin, B. J., and Ervasti, J. M. (2010) The actin gene family: function follows isoform. *Cytoskeleton (Hoboken)* 67, 630-634

37. Peckham, M., Miller, G., Wells, C., Zicha, D., and Dunn, G. A. (2001) Specific changes to the mechanism of cell locomotion induced by overexpression of beta-actin. *J Cell Sci* 114, 1367-1377

38. Karakozova, M., Kozak, M., Wong, C. C., Bailey, A. O., Yates, J. R., 3rd, Mogilner, A., Zebroski, H., and Kashina, A. (2006) Arginylation of beta-actin regulates actin cytoskeleton and cell motility. *Science* 313, 192-196

39. Zhang, F., Saha, S., Shabalina, S. A., and Kashina, A. (2010) Differential arginylation of actin isoforms is regulated by coding sequence-dependent degradation. *Science* 329, 1534-1537

40. Schevzov, G., Lloyd, C., and Gunning, P. (1992) High level expression of transfected beta- and gamma-actin genes differentially impacts on myoblast cytoarchitecture. *J Cell Biol* 117, 775-785

41. Harborth, J., Elbashir, S. M., Bechert, K., Tuschl, T., and Weber, K. (2001) Identification of essential genes in cultured mammalian cells using small interfering RNAs. *J Cell Sci* 114, 4557-4565

42. Shawlot, W., Deng, J. M., Fohn, L. E., and Behringer, R. R. (1998) Restricted beta-galactosidase expression of a hygromycin-lacZ gene targeted to the beta-actin locus and embryonic lethality of beta-actin mutant mice. *Transgenic Res* 7, 95-103

43. Shmerling, D., Danzer, C. P., Mao, X., Boisclair, J., Haffner, M., Lemaistre, M., Schuler, V., Kaeslin, E., Korn, R., Burki, K., Ledermann, B., Kinzel, B., and Muller, M. (2005) Strong and ubiquitous expression of transgenes targeted into the beta-actin locus by Cre/lox cassette replacement. *Genesis* 42, 229-235

44. Sonnemann, K. J., Fitzsimons, D. P., Patel, J. R., Liu, Y., Schneider, M. F., Moss, R. L., and Ervasti, J. M. (2006) Cytoplasmic gamma-actin is not required for skeletal muscle development but its absence leads to a progressive myopathy. *Dev Cell* 11, 387-397

45. Belyantseva, I. A., Perrin, B. J., Sonnemann, K. J., Zhu, M., Stepanyan, R., McGee, J., Frolenkov, G. I., Walsh, E. J., Friderici, K. H., Friedman, T. B., and Ervasti, J. M. (2009) Gamma-actin is required for cytoskeletal maintenance but not development. *Proc Natl Acad Sci U S A* 106, 9703-9708

46. Furness, D. N., Katori, Y., Mahendrasingam, S., and Hackney, C. M. (2005) Differential distribution of beta- and gamma-actin in guinea-pig cochlear sensory and supporting cells. *Hear Res* 207, 22-34

47. Yao, X., Chaponnier, C., Gabbiani, G., and Forte, J. G. (1995) Polarized distribution of actin isoforms in gastric parietal cells. *Mol Biol Cell* 6, 541-557

48. Jacinto, A., and Baum, B. (2003) Actin in development. *Mech Dev* 120, 1337-1349

49. Copp, A. J., Greene, N. D., and Murdoch, J. N. (2003) The genetic basis of mammalian neurulation. *Nat Rev Genet* 4, 784-793

50. Kaufman, M. H. (1992) *The Atlas of Mouse Development*, Elsevier Academic Press, London

51. Anderson, R. H., Webb, S., Brown, N. A., Lamers, W., and Moorman, A. (2003) Development of the heart: (3) formation of the ventricular outflow tracts, arterial valves, and intrapericardial arterial trunks. *Heart* 89, 1110-1118

52. Lloyd, C., Schevzov, G., and Gunning, P. (1992) Transfection of nonmuscle beta- and gamma-actin genes into myoblasts elicits different feedback regulatory responses from endogenous actin genes. *J Cell Biol* 117, 787-797

53. Vartiainen, M. K., Guettler, S., Larijani, B., and Treisman, R. (2007) Nuclear actin regulates dynamic subcellular localization and activity of the SRF cofactor MAL. *Science* 316, 1749-1752

54. Busche, S., Descot, A., Julien, S., Genth, H., and Posern, G. (2008) Epithelial cell-cell contacts regulate SRF-mediated transcription via Rac-actin-MAL signalling. *J Cell Sci* 121, 1025-1035

55. Franklin-Tong, V. E., and Gourlay, C. W. (2008) A role for actin in regulating apoptosis/programmed cell death: evidence spanning yeast, plants and animals. *Biochem J* 413, 389-404

56. Otey, C. A., Kalnoski, M. H., Lessard, J. L., and Bulinski, J. C. (1986) Immunolocalization of the gamma isoform of nonmuscle actin in cultured cells. *J Cell Biol* 102, 1726-1737

57. van Wijk, E., Krieger, E., Kemperman, M. H., De Leenheer, E. M., Huygen, P. L., Cremers, C. W., Cremers, F. P., and Kremer, H. (2003) A mutation in the gamma actin 1 (ACTG1) gene causes autosomal dominant hearing loss (DFNA20/26). *J Med Genet* 40, 879-884

58. Zhu, M., Yang, T., Wei, S., DeWan, A. T., Morell, R. J., Elfenbein, J. L., Fisher, R. A., Leal, S. M., Smith, R. J., and Friderici, K. H. (2003) Mutations in the gamma-actin gene (ACTG1) are associated with dominant progressive deafness (DFNA20/26). *Am J Hum Genet* 73, 1082-1091

59. Shuster, C. B., Lin, A. Y., Nayak, R., and Herman, I. M. (1996) Beta cap73: a novel beta actin-specific binding protein. *Cell Motil Cytoskeleton* 35, 175-187

60. Tzima, E., Trotter, P. J., Orchard, M. A., and Walker, J. H. (2000) Annexin V relocates to the platelet cytoskeleton upon activation and binds to a specific isoform of actin. *Eur J Biochem* 267, 4720-4730

61. Bergeron, S. E., Zhu, M., Thiem, S. M., Friderici, K. H., and Rubenstein, P. A. (2010) Ion-dependent polymerization differences between mammalian beta- and gamma-nonmuscle actin isoforms. *J Biol Chem* 285, 16087-16095

62. Bunnell, T. M., and Ervasti, J. M. (2010) Delayed embryonic development and impaired cell growth and survival in Actg1 null mice. *Cytoskeleton (Hoboken)* 67, 564-572

63. Perrin, B. J., Sonnemann, K. J., and Ervasti, J. M. (2010) beta-Actin and gamma-Actin Are Each Dispensable for Auditory Hair Cell Development But Required for Stereocilia Maintenance. *PLoS Genet* 6, e1001158

64. Condeelis, J., and Singer, R. H. (2005) How and why does beta-actin mRNA target? *Biol Cell* 97, 97-110

65. Kashina, A. S. (2006) Differential arginylation of actin isoforms: the mystery of the actin N-terminus. *Trends Cell Biol* 16, 610-615

66. Holzenberger, M., Lenzner, C., Leneuve, P., Zaoui, R., Hamard, G., Vaulont, S., and Bouc, Y. L. (2000) Cre-mediated germline mosaicism: a method allowing rapid generation of several alleles of a target gene. *Nucleic Acids Res* 28, E92

67. Hayashi, S., and McMahon, A. P. (2002) Efficient recombination in diverse tissues by a tamoxifen-inducible form of Cre: a tool for temporally regulated gene activation/inactivation in the mouse. *Dev Biol* 244, 305-318

68. Hinz, B., Alt, W., Johnen, C., Herzog, V., and Kaiser, H. W. (1999) Quantifying lamella dynamics of cultured cells by SACED, a new computer-assisted motion analysis. *Exp Cell Res* 251, 234-243

69. Farina, K. L., Huttelmaier, S., Musunuru, K., Darnell, R., and Singer, R. H. (2003) Two ZBP1 KH domains facilitate beta-actin mRNA localization, granule formation, and cytoskeletal attachment. *J Cell Biol* 160, 77-87

70. Ronnov-Jessen, L., and Petersen, O. W. (1996) A function for filamentous alpha-smooth muscle actin: retardation of motility in fibroblasts. *J Cell Biol* 134, 67-80

71. Nunoi, H., Yamazaki, T., Tsuchiya, H., Kato, S., Malech, H. L., Matsuda, I., and Kanegasaki, S. (1999) A heterozygous mutation of beta-actin associated with neutrophil dysfunction and recurrent infection. *Proc Natl Acad Sci U S A* 96, 8693-8698

72. Procaccio, V., Salazar, G., Ono, S., Styers, M. L., Gearing, M., Davila, A., Jimenez, R., Juncos, J., Gutekunst, C. A., Meroni, G., Fontanella, B., Sontag, E., Sontag, J. M., Faundez, V., and Wainer, B. H. (2006) A mutation of beta -actin that alters depolymerization dynamics is associated with autosomal dominant developmental malformations, deafness, and dystonia. *Am J Hum Genet* 78, 947-960

73. Gearing, M., Juncos, J. L., Procaccio, V., Gutekunst, C. A., Marino-Rodriguez, E. M., Gyure, K. A., Ono, S., Santoianni, R., Krawiecki, N. S., Wallace, D. C., and Wainer, B. H. (2002) Aggregation of actin and cofilin in identical twins with juvenile-onset dystonia. *Ann Neurol* 52, 465-476

74. Le, P. U., Nguyen, T. N., Drolet-Savoie, P., Leclerc, N., and Nabi, I. R. (1998) Increased beta-actin expression in an invasive moloney sarcoma virus-transformed MDCK cell variant concentrates to the tips of multiple pseudopodia. *Cancer Res* 58, 1631-1635

75. Nowak, D., Skwarek-Maruszewska, A., Zemanek-Zboch, M., and Malicka-Blaszkiewicz, M. (2005) Beta-actin in human colon adenocarcinoma cell lines with different metastatic potential. *Acta Biochim Pol* 52, 461-468

76. Popow, A., Nowak, D., and Malicka-Blaszkiewicz, M. (2006) Actin cytoskeleton and beta-actin expression in correlation with higher invasiveness of selected hepatoma Morris 5123 cells. *J Physiol Pharmacol* 57 Suppl 7, 111-123

77. Lee, P. P., Fitzpatrick, D. R., Beard, C., Jessup, H. K., Lehar, S., Makar, K. W., Perez-Melgosa, M., Sweetser, M. T., Schlissel, M. S., Nguyen, S., Cherry, S. R., Tsai, J. H., Tucker, S. M., Weaver, W. M., Kelso, A., Jaenisch, R., and Wilson, C. B. (2001) A critical role for Dnmt1 and DNA methylation in T cell development, function, and survival. *Immunity* 15, 763-774

78. Fujii, T., Iwane, A. H., Yanagida, T., and Namba, K. (2010) Direct visualization of secondary structures of F-actin by electron cryomicroscopy. *Nature* 467, 724-728

79. Larsson, H., and Lindberg, U. (1988) The effect of divalent cations on the interaction between calf spleen profilin and different actins. *Biochim Biophys Acta* 953, 95-105

80. Ohshima, S., Abe, H., and Obinata, T. (1989) Isolation of profilin from embryonic chicken skeletal muscle and evaluation of its interaction with different actin isoforms. *J Biochem* 105, 855-857

81. Weber, A., Nachmias, V. T., Pennise, C. R., Pring, M., and Safer, D. (1992) Interaction of thymosin beta 4 with muscle and platelet actin: implications for actin sequestration in resting platelets. *Biochemistry* 31, 6179-6185

82. Namba, Y., Ito, M., Zu, Y., Shigesada, K., and Maruyama, K. (1992) Human T cell L-plastin bundles actin filaments in a calcium-dependent manner. *J Biochem* 112, 503-507

83. Yao, X., Cheng, L., and Forte, J. G. (1996) Biochemical characterization of ezrin-actin interaction. *J Biol Chem* 271, 7224-7229

84. De La Cruz, E. M. (2005) Cofilin binding to muscle and non-muscle actin filaments: isoform-dependent cooperative interactions. *J Mol Biol* 346, 557-564

85. Zhao, K., Wang, W., Rando, O. J., Xue, Y., Swiderek, K., Kuo, A., and Crabtree, G. R. (1998) Rapid and phosphoinositol-dependent binding of the SWI/SNF-like BAF complex to chromatin after T lymphocyte receptor signaling. *Cell* 95, 625-636

86. Ikura, T., Ogryzko, V. V., Grigoriev, M., Groisman, R., Wang, J., Horikoshi, M., Scully, R., Qin, J., and Nakatani, Y. (2000) Involvement of the TIP60 histone acetylase complex in DNA repair and apoptosis. *Cell* 102, 463-473

87. Hofmann, W. A., Stojiljkovic, L., Fuchsova, B., Vargas, G. M., Mavrommatis, E., Philimonenko, V., Kysela, K., Goodrich, J. A., Lessard, J. L., Hope, T. J., Hozak, P., and de Lanerolle, P. (2004) Actin is part of pre-initiation complexes and is necessary for transcription by RNA polymerase II. *Nat Cell Biol* 6, 1094-1101

88. Hu, P., Wu, S., and Hernandez, N. (2004) A role for beta-actin in RNA polymerase III transcription. *Genes Dev* 18, 3010-3015

89. Hinz, B. (2010) The myofibroblast: paradigm for a mechanically active cell. *J Biomech* 43, 146-155

Appendix

Destabilization of the Dystrophin-Glycoprotein Complex without Functional Deficits in α-Dystrobrevin Null Muscle

My thesis work stemmed from my initial interest in investigating unique roles for each cytoplasmic actin isoform in mammalian development. Since developmental biology was a new area of scientific research for the Ervasti laboratory, I had decided to take on an additional "backup" project that more closely aligned with established areas of research in the Ervasti laboratory. As such, I investigated the biochemical stability of the dystrophin-glycoprotein complex as well as muscle performance in α-dystrobrevin null mice, a previously reported dystrophic mouse model exhibiting extensive myofiber degeneration. This investigation led to the surprising conclusion that instability of the dystrophin-glycoprotein complex and myofiber degeneration do not necessarily lead to altered muscle performance. This work was co-authored with a fellow graduate student, Michele Jaeger, and published in *PLoS One*.

The following report is unmodified from the published article:

Bunnell, T.M.[1], Jaeger, M.A.[1], Fitzsimons, D.P., Prins, K.W., Ervasti, J.M. (2008) Destabilization of the dystrophin-glycoprotein complex without functional deficits in α-dystrobrevin null muscle. *PLoS One* 3(7):e2604

[1] Both authors contributed equally to this work.

Tina Bunnell performed the biochemical and whole-body tension experiments, as well as analyzed the *ex vivo* force measurement data. Michele Jaeger performed the histological and immunofluorescence analyses. Dan Fitzsimons performed the *ex vivo* force measurements. Kurt Prins performed the treadmill exhaustion study. Tina Bunnell and Michele Jaeger co-wrote the manuscript.

α-Dystrobrevin is a component of the dystrophin-glycoprotein complex (DGC) and is thought to have both structural and signaling roles in skeletal muscle. Mice deficient for α-dystrobrevin (*adbn*$^{-/-}$) exhibit extensive myofiber degeneration and neuromuscular junction abnormalities. However, the biochemical stability of the DGC and the functional performance of *adbn*$^{-/-}$ muscle have not been characterized. Here we show that the biochemical association between dystrophin and β-dystroglycan is compromised in *adbn*$^{-/-}$ skeletal muscle, suggesting that α-dystrobrevin plays a structural role in stabilizing the DGC. However, despite muscle cell death and DGC destabilization, costamere organization and physiological performance is normal in *adbn*$^{-/-}$ skeletal muscle. Our results demonstrate that myofiber degeneration alone does not cause functional deficits and suggests that more complex pathological factors contribute to the development of muscle weakness in muscular dystrophy.

Introduction

The dystrophin-glycoprotein complex (DGC) is comprised of dystrophin, the dystroglycans (α and β), the sarcoglycans (α, β, γ and δ), sarcospan, the syntrophins (α1, β1, β2) and α-dystrobrevin [1]. In skeletal muscle, this large complex of membrane-associated proteins links the sub-sarcolemmal actin cytoskeleton to the extracellular matrix and is thought to provide protection from stresses imposed during muscle contraction [2]. Mutations in several DGC components result in muscular dystrophy in both humans and a variety of animal models. Dystrophin is one of the best characterized DGC proteins and its absence in humans and the *mdx* mouse leads to a destabilization of the DGC, sarcolemmal fragility, myofiber degeneration and muscle weakness [3]. The absence of functional sarcoglycans (α-β-γ-and δ-) or dystroglycan also result in muscular dystrophies with similar pathological features [4–6].

α-Dystrobrevin is a dystrophin-related protein that binds directly to dystrophin, syntrophin, and the sarcoglycan complex [7–10]. In addition, α-dystrobrevin binds to the intermediate filament proteins syncoilin and synemin, thereby linking the DGC to the intermediate filament network [11,12]. The importance of α-dystrobrevin in maintaining healthy muscle is demonstrated by the α-dystrobrevin null (*adbn*$^{-/-}$) mouse, which exhibits extensive myofiber degeneration [13]. However, several important questions remain regarding the function of α-dystrobrevin and the relationship of the *adbn*$^{-/-}$ muscle phenotype to other dystrophic animal models. In particular, whether the absence of α-dystrobrevin leads to DGC instability or causes deficits in muscle function remain to be assessed.

To further investigate the consequences of α-dystrobrevin deficiency, we examined the biochemical stability of the DGC and also measured the *in vivo* and *ex vivo* physiological performance of *adbn*$^{-/-}$ muscle. Our results suggest that the interaction between dystrophin and β-dystroglycan is compromised by the loss of α-dystrobrevin, implicating a role for α-dystrobrevin in stabilizing the DGC. However, muscle function was not compromised in *adbn*$^{-/-}$ mice, which demonstrates that substantial muscle cell necrosis can occur without adverse effect on physiological performance.

Materials and Methods

Animals

A breeding pair of *adbn*$^{-/-}$ mice was generously provided by Dr. R. Mark Grady (Washington University, St. Louis, MO). To generate *adbn*$^{+/-}$ mice for controls, we outcrossed an *adbn*$^{-/-}$ male (SV129J/ C57Bl/6J mixed background) to an SV129J wild-type female to obtain *adbn*$^{+/-}$ mice. Subsequent mating between *adbn*$^{+/-}$ and *adbn*$^{-/-}$ mice provided *adbn*$^{-/-}$ and littermate control *adbn*$^{+/-}$ animals. Genotypic analyses were performed by standard PCR methods.

Light and Confocal Microscopy

For light microscopy, muscles were dissected from *adbn*$^{-/-}$ and *adbn*$^{+/-}$ 7 month-old mice, quickly frozen in liquid nitrogen-cooled isopentane and mounted in O.C.T medium (TissueTek, Torrance, CA). 10 μm cryosections were cut on a Leica CM3050 cryostat, air-dried and stained with hematoxylin and eosin-phloxine. Images were obtained on a Zeiss Axiovert 25 microscope fitted with a Leica DFC300 FX camera using Image Pro Plus 5.1 software.

Costamere images were obtained according to previously described methods [23]. Mice were trans-cardially perfused with ice-cold 2% paraformaldehyde in phosphate buffered saline (PBS). Quadriceps were dissected, adhered to a cryostat chuck with O.C.T. medium and quickly frozen in liquid-nitrogen slush. 20 μm longitudinal cryosections were cut and stored at -80°C. For confocal microscopy, sections were thawed, blocked for 30 minutes in PBS/BSA (PBS containing 1 mg/ml bovine serum albumin and 10 mM NaN_3) and incubated with a 1:100 dilution of Rabbit 2 polyclonal

antibody to dystrophin [25] for 2 hours at room temperature. Sections were rinsed with PBS/BSA, incubated with 1:200 Alexa-488-conjugated 2° antibody (Molecular Probes, Carlsbad, CA) for 30 minutes at room temperature and rinsed with PBS/BSA. To visualize nuclei, 8 μM TO-PRO 3 iodide (Molecular Probes, Carlsbad, CA) was applied to sections for 5 minutes, rinsed with PBS/BSA and a coverslip applied with a drop of Slow-Fade Reagent (Molecular Probes, Carlsbad, CA). Slides were viewed on an Olympus Fluoview 1000 inverted confocal microscope with a 60x (NA 1.4) oil objective at the University of Minnesota-Twin Cities Biomedical Imaging Processing Laboratory. Laser power and PMT voltage were adjusted so that 2° antibody alone did not produce signal.

Biochemical Analysis of DGC Stability

Skeletal muscle was dissected, snap-frozen in liquid nitrogen, and pulverized in a liquid nitrogen-cooled mortar and pestle. Total muscle homogenates were prepared by solubilizing pulverized muscle in 1% SDS, 5 mM EGTA, and protease inhibitors for 2 minutes at 100°C. The supernatant was collected after brief centrifugation and its protein concentration determined using the Bio-Rad *DC* Protein Assay Kit II (Bio-Rad, Hercules, CA). To enrich for the DGC, pulverized muscle was solubilized in 10 volumes/g of 50 mM Tris-HCl, 0.5 M NaCl, 1% digitonin and a cocktail of protease inhibitors for 1 hour at 4°C with gentle mixing. After high-speed centrifugation, the supernatant was applied to a WGA-Sepharose column (Sigma-Aldrich, St. Louis, MO) pre-equilibrated with wash buffer (50 mM Tris-HCl, 0.5 M NaCl, 0.1% digitonin, and protease inhibitors) for 2 hours at 4°C to enrich for dystroglycan and associated proteins. The column was washed

and bound proteins eluted with Laemmli sample buffer (3% SDS and 1% β-mercaptoethanol) at 100°C. Dystrophin and β-dystroglycan immunoreactivity in SDS muscle solubilates (50 μg total protein) and WGA elutes were measured by quantitative western blot analysis using the monoclonal antibodies NCL-DYS1 to dystrophin and NCL-b-DG to β-dystroglycan (Novocastra Laboratories Ltd, Newcastle upon Tyne, UK). Secondary antibodies were IRDye 800- or IRDye680-conjugated goat anti-mouse IgG and the fluorescent signals were detected and quantified using the Odyssey Infrared Imaging System (LI-COR Biosciences, Lincoln, NE). Relative levels of dystrophin from WGA elutes were determined by normalizing dystrophin signals to the corresponding β-dystroglycan signal. Statistical significance at $p<0.05$ was determined using a one-sample t-test.

Ex Vivo Force Measurements

All force measurements were obtained as previously described [43] from both male and female mice at 2 and 7 months of age. Experiments were conducted on both the right and left EDL muscle for each mouse. The EDL muscle was dissected and one tendon attached to a rigid support and the other to a dual-mode servomotor. The muscle was allowed to equilibrate in a Ca^{2+}-Ringer's solution continuously gassed with 95% O_2/5% CO_2 to maintain a pH of 7.6 at 30°C. Platinum plate electrodes were positioned on either side of the muscle and stimulation induced by a single pulse lasting 200 microseconds. The muscle was adjusted to the optimal length (L_0) at which maximal twitch force was achieved. Muscle was then subjected to an ECC regimen which consisted of five maximal tetanic stimulations at a frequency of 150 Hertz. Each

stimulation was carried out over 700 milliseconds; over the final 200 milliseconds the muscle was lengthened at a velocity of 0.5 L_0/second resulting in a total stretch of 10% L_0. A five-minute recovery time was allowed between measurements. The average force produced during a stretch was calculated by integrating the force-time curve and dividing this value by the duration of the stretch. Work was calculated by multiplying the average force produced during a stretch by the length of the displacement and normalized to muscle mass. Upon completion of the ECC protocol, muscle was weighed and subsequently bathed in 0.1% Procion orange, washed, and frozen for cryosectioning. Cross sectional area of each muscle was calculated according to Brooks and Faulkner [44] by dividing muscle wet mass by the product of L_0, the EDL fiber-to-muscle length constant 0.44, and 1.06 grams/centimeter^3, the density of mammalian skeletal muscle [44]. Differences between genotypes at each time point were assessed by using a Student's two-tailed t-test for independent samples to determine significance at $p<0.05$.

In Vivo Physiological Performance

The WBT protocol was carried out as previously described [43]. A mouse was attached by the tail to a horizontally mounted force transducer using suture silk and subsequently placed in an apparatus that allowed only forward movement. The force evoked by gentle tail pinches (approximately 5 pinches per minute) was recorded for 5 minutes and the top 5 values were identified and normalized to body mass.

Maximal exercise performance was tested on a Columbus Instruments treadmill with an uphill grade of 15°. Mice were acclimated to the treadmill by running at a speed of 10 meters per minute for 5 minutes, three times a week, for two weeks. To determine

maximal exercise performance mice were run on the treadmill for 5 minutes, at a speed of 10 meters per minute, followed by a 1 meter per minute increase in speed every minute until exhaustion. Mice were considered exhausted when they refused to stay off a shock bar for at least 5 seconds. Maximal exercise capacity was determined as the average duration of two trials separated by two days. Differences between *adbn*$^{+/-}$ and *adbn*$^{-/-}$ mice at each time point were assessed by using a Student's two-tailed t-test for independent samples to determine significance at $p<0.05$.

Results

α-dystrobrevin biochemically stabilizes the DGC

We first assessed general histopathology by performing hematoxylin and eosin-phloxine staining on quadriceps, gastrocnemius and tibialis anterior muscles from 7 month old *adbn*$^{+/-}$ and *adbn*$^{-/-}$ mice (Figure 1; tibialis anterior muscle not shown). Consistent with the findings of Grady et al. [13], *adbn*$^{-/-}$ skeletal muscle exhibited pockets of centrally-nucleated fibers, indicating that muscle degeneration and regeneration had occurred. Overall, approximately 50% of the fibers contained central nuclei in all muscle types examined. However, unlike other animal models in which DGC components have been ablated [14–20], we observed no evidence of fibrosis, mononuclear cell infiltration or adipose deposition.

Previous work implicated α-dystrobrevin as a linker protein between dystrophin and the sarcoglycan complex [10]. To assess whether α-dystrobrevin may play a structural role within the DGC, we measured the biochemical stability of the dystrophin-dystroglycan interaction in *adbn*$^{-/-}$ mice. Since it was initially reported that *adbn*$^{-/-}$ mice exhibit a progressive myopathy [13] we measured the biochemical stability of the DGC at both 2 and 7 months of age. Western blot analysis of SDS homogenates confirmed the absence of α-dystrobrevin in *adbn*$^{-/-}$ muscle (Figure 2A). Total muscle lysates from *adbn*$^{+/-}$ and *adbn*$^{-/-}$ muscle also exhibited comparable levels of dystrophin (Figure 2A) and β-dystroglycan (data not shown), consistent with reports from Grady et al. [21]. However, upon enrichment of the DGC from digitonin-solubilized muscle by wheat germ agglutinin (WGA) chromatography [22], dystrophin immunoreactivity in *adbn*$^{-/-}$ muscle

was significantly reduced to 26% and 30% of that in *adbn*$^{+/-}$ muscle at 2 and 7 months of age, respectively (Figure 2B-C). These data indicate that the biochemical interaction of dystrophin with the dystroglycan complex is compromised in the absence of α-dystrobrevin.

Costameres are structurally normal in adbn$^{-/-}$ muscle

It was previously shown that the dystrophin-deficient *mdx* mouse exhibits altered costamere organization [23,24] and impaired costamere anchorage to the sarcolemma [25]. In addition to its association with dystrophin, α-dystrobrevin interacts both directly and indirectly with several intermediate filament proteins within the costameric network [11,12]. Similar to the *mdx* mouse, mice deficient for desmin, an intermediate filament protein that interacts indirectly with α-dystrobrevin via its association with syncoilin [11,26], display a loss of costamere structure in certain muscles [27]. Given that α-dystrobrevin interacts with proteins necessary for proper costamere formation and stabilizes the DGC (Figure 2), we investigated costamere organization in *adbn*$^{-/-}$ mice. Both wild-type and *adbn*$^{-/-}$ skeletal muscle at 7 months of age exhibited highly organized rectilinear costamere structures with predominate dystrophin staining at the Z-line, finer transverse elements in register with the M-line and longitudinal elements (Figure 3). These results indicate that α-dystrobrevin is not required for proper costamere organization.

Physiological performance is normal in adbn$^{-/-}$ mice

To investigate the functional consequences of DGC instability (Figure 2) and muscle cell death (Figure 1) in *adbn*$^{-/-}$ mice, we assessed *ex vivo* and *in vivo* physiological

performance using established techniques. Contractile properties of isolated extensor digitorum longus (EDL) muscles from *adbn*$^{+/-}$ and *adbn*$^{-/-}$ mice were determined at 2 and 7 months of age (Table 1). At both ages, isometric twitch force and specific force did not significantly differ between control and null muscle. Furthermore, *adbn*$^{-/-}$ muscle did not show an increased force drop after four eccentric contractions (ECCs). Since work done to stretch the muscle is the best predictor of the magnitude of contraction-induced injury [28], we calculated the combined work from all four ECCs and did not observe a significant difference between *adbn*$^{+/-}$ and *adbn*$^{-/-}$ muscle. In addition, we did not see an increase in Procion orange infiltration of *adbn*$^{-/-}$ myofibers compared to control after eccentric contractions (data not shown), indicating that sarcolemmal stability is not affected in *adbn*$^{-/-}$ muscle.

Total body strength was assessed by measuring whole-body tension (WBT), defined as the forward pulling tension exerted by an individual mouse in response to a tail pinch stimulus [29]. Maximal responses (WBT_1) and the average of the top five responses (WBT_{1-5}) did not differ between *adbn*$^{+/-}$ and *adbn*$^{-/-}$ animals at either 2 or 7 months of age (Figure 4A). To evaluate the endurance capacity of *adbn*$^{-/-}$ mice, maximal exercise performance tests were carried out using an uphill treadmill running regimen. At 7 months of age *adbn*$^{-/-}$ mice displayed similar times to exhaustion as *adbn*$^{+/-}$ mice (Figure 4B). Together, these data demonstrate that despite biochemical destabilization of the DGC and substantial muscle necrosis, *adbn*$^{-/-}$ mice exhibit normal skeletal muscle function.

Figure 1: Histology of *adbn*$^{+/-}$ and *adbn*$^{-/-}$ muscle. Shown are representative hematoxylin and eosin stained sections of quadriceps and gastrocnemius muscle from 7 month *adbn*$^{+/-}$ and *adbn*$^{-/-}$ mice. Focal areas of centrally-nucleated fibers are evident throughout *adbn*$^{-/-}$ muscles, indicative of myofiber degeneration and regeneration.

Figure 1

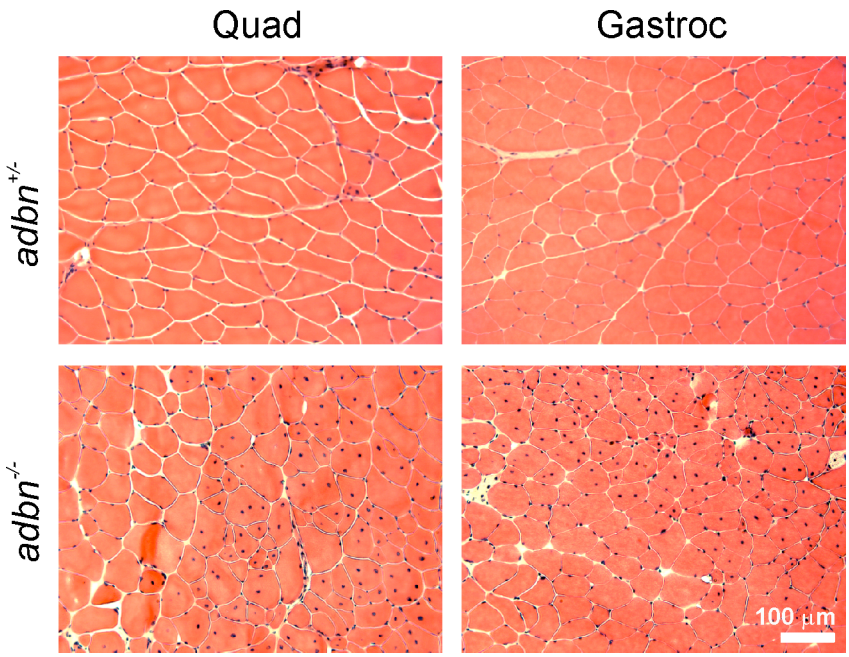

Figure 2: α-Dystrobrevin biochemically stabilizes the DGC. A: Representative immunoblots for α-dystrobrevin and dystrophin from SDS-solubilized skeletal muscle. **B:** Representative immunoblots for β-dystroglycan and dystrophin from digitonin-solubilized skeletal muscle enriched for the DGC using WGA-chromatography. **C:** Quantification of the relative levels of dystrophin, after normalizing to β-dystroglycan intensity, from muscle solubilates incubated with WGA-agarose beads. Asterisks denotes a significant (one-sample t-test, $p < 0.05$) reduction in the levels of dystrophin. $n = 3$ for each genotype/time point; error bars represent s.e.m.

Figure 2

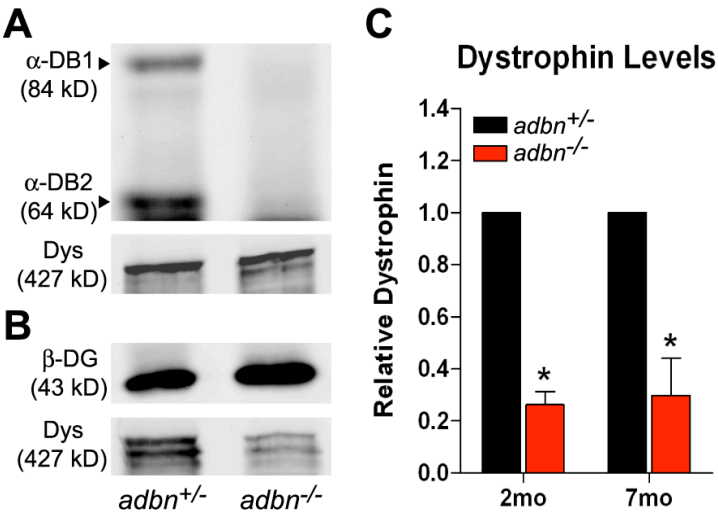
A
α-DB1
(84 kD)
α-DB2
(64 kD)
Dys
(427 kD)
B
β-DG
(43 kD)
Dys
(427 kD)
adbn+/-
adbn-/-
C
Dystrophin Levels
adbn+/-
adbn-/-
Relative Dystrophin
1.4
1.2
1.0
0.8
0.6
0.4
0.2
0.0
*
*
2mo
7mo

Figure 3: Normal costameres in *adbn*$^{-/-}$ muscle. Longitudinal cryosections of quadriceps from 7 month old mice stained with Rabbit 2 polyclonal antibody to dystrophin. Nuclei are stained blue.

Figure 3

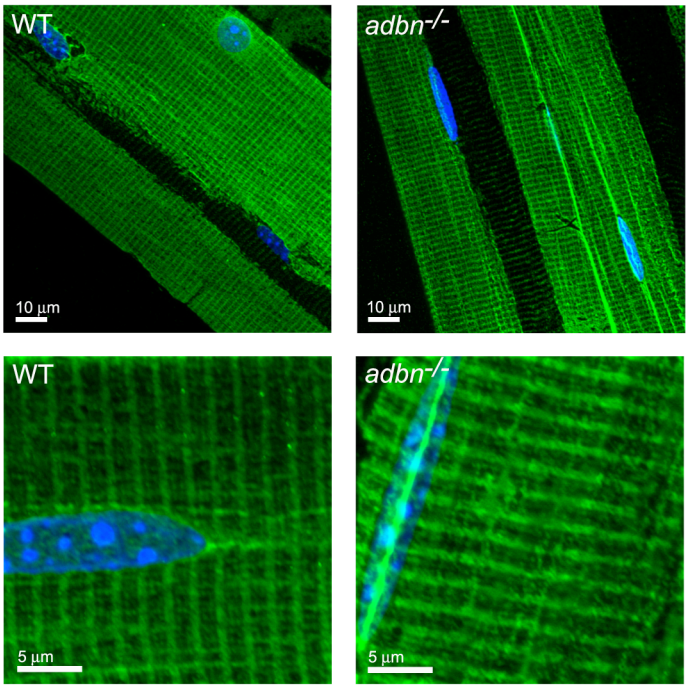

Table 1. Morphometric and contractile properties of EDL muscle.

	2 months		7 months	
	***adbn*$^{+/-}$**	***adbn*$^{-/-}$**	***adbn*$^{+/-}$**	***adbn*$^{-/-}$**
Parameter	n=3	n=3	n=6	n=6
L_o (mm)	11.3 ± 0.3	11.5 ± 0.5	12.5 ± 0.2	12.0 ± 0.2
EDL mass (mg)	12.2 ± 1.7	10.4 ± 1.4	12.4 ± 0.8	11.4 ± 0.6
TPT (ms)	7.8 ± 0.4	7.8 ± 0.2	9.9 ± 0.5	10.1 ± 0.6
$RT_{1/2}$ (ms)	8.3 ± 1.8	11.3 ± 3.1	13.1 ± 0.9	12.5 ± 0.7
Twitch force (mN)	22.0 ± 4.0	28.6 ± 7.9	45.0 ± 5.1	34.1 ± 4.0
Twitch force (mN/mm^2)	10.4 ± 2.7	14.5 ± 2.8	22.2 ± 3.8	16.7 ± 1.7
Tetanic force (mN)	238.2 ± 38.2	247.3 ± 46.3	395.2 ± 8.3	340.0 ± 28.6
Tetanic force (mN/mm^2)	111.4 ± 27.3	127.1 ± 12.7	190.1 ± 15.8	166.1 ± 8.6
Force drop (%)	24.1 ± 4.3	33.0 ± 8.6	20.5 ± 1.8	22.0 ± 4.8
Work (J/kg)	136.6 ± 30.8	167.9 ± 13.6	213.1 ± 17.0	197.2 ± 7.0

Results are presented as mean ± s.e.m.

TPT, time to peak tension; $RT_{1/2}$, half relaxation time

Figure 4: *adbn*$^{-/-}$ mice exhibit normal physiological performance *in vivo*. A: Whole-body tension analysis depicting averages of the maximal response (WBT_1) and the top five responses (WBT_{1-5}) at 2 and 7 months of age. $n \geq 3$ for each genotype/time point. **B:** Time to exhaustion during uphill treadmill running at 7 months of age. $n = 4$ for each genotype. No significant differences were observed. Error bars represent s.e.m.

Figure 4

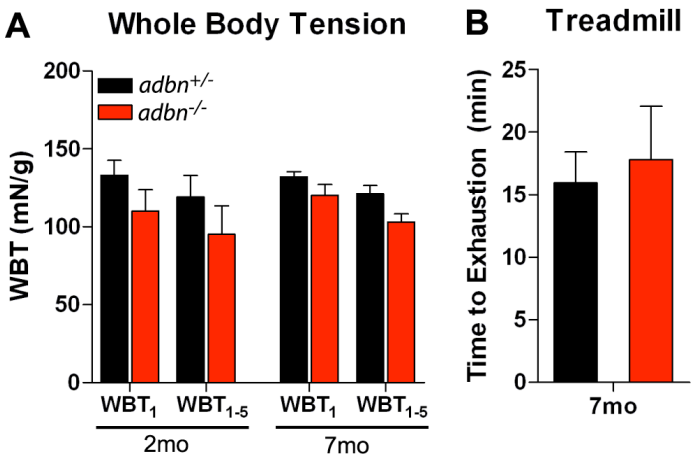
A
Whole Body Tension
B
Treadmill
WBT (mN/g)
200
150
100
50
0
adbn+/-
adbn-/-
WBT1
WBT1-5
WBT1
WBT1-5
2mo
7mo
Time to Exhaustion (min)
25
20
15
10
5
0
7mo

Discussion

Since the initial observation that *adbn*$^{-/-}$ mice exhibit skeletal and cardiac muscle cell necrosis [13], the *adbn*$^{-/-}$ mouse has been considered an animal model for muscular dystrophy. However, as muscular dystrophy is characterized by both muscle cell death and muscle weakness, we examined the functional performance of *adbn*$^{-/-}$ muscle. Surprisingly, *adbn*$^{-/-}$ muscle was indistinguishable from control muscle using both *in vivo* and *ex vivo* analyses. These results were unanticipated, as *adbn*$^{-/-}$ mice exhibit an elevated presence of centrally-nucleated fibers similar to other mouse models of muscular dystrophy [13]. Although the exact cause(s) of muscle cell death and weakness in muscular dystrophy remains to be determined, it is reasonable to postulate that cell death contributes to the development of muscle weakness. Our results suggest that a more complex pathomechanism underlies the decreased physiological performance associated with muscular dystrophies.

Some fundamental differences in the histological observations between *adbn*$^{-/-}$ mice and other DGC-associated muscular dystrophy mouse models may help to explain the lack of a functional deficit in *adbn*$^{-/-}$ mice. Unlike muscle from dystrophin-, sarcoglycan- and dystroglycan-deficient animals [14–20], *adbn*$^{-/-}$ muscle does not exhibit significant fibrosis, mononuclear cell infiltration or increased membrane damage. Therefore, fibrosis, inflammation and membrane fragility may be factors contributing to the force deficits observed in dystrophic animal models. In fact, replacement of muscle fibers with less elastic fibrotic connective tissue has previously been suggested to contribute to decreased force production [30]. Furthermore, treatment of dystrophic mice

and humans with corticosteroids, which is believed to help reduce inflammation, improves muscle function [31,32], supporting the idea that inflammation also contributes to muscle weakness.

While the cause of muscle cell death in DGC-related muscular dystrophies is unclear, a leading hypothesis is that damage to the sarcolemma during muscle contraction causes a loss of calcium homeostasis, leading to activation of proteases and eventual cell death [33]. However, similar to our findings in *adbn*$^{-/-}$ mice, Warner et al. [34] report that Dp260/*mdx* mice exhibit muscle cell necrosis in the absence of sarcolemmal damage. These results indicate that sarcolemmal instability is not the sole cause of cell death. In the absence of sarcolemmal fragility, it has been hypothesized that cell death in *adbn*$^{-/-}$ mice results from aberrant signaling. Grady et al. [13] demonstrated a loss of sarcolemmal-localized neuronal nitric oxide synthase (nNOS) and impaired nNOS signaling in *adbn*$^{-/-}$ mice [13]. Impaired nNOS signaling leads to vasoconstriction and thereby decreased blood flow in active muscle [35]. Such ischemic conditions could explain the focal areas of necrosis observed in *adbn*$^{-/-}$ mice, which is similar to the histology of δ-sarcoglycan null mice in which vascular function is perturbed [36]. However, the loss of nNOS alone is unlikely to account for the dystrophy in *adbn*$^{-/-}$ mice since nNOS-deficient mice are not detectably dystrophic [37]. The question therefore remains as to what causes cell death in the absence of sarcolemmal damage. Understanding the mechanism underlying muscle degeneration in *adbn*$^{-/-}$ mice may provide insight into the molecular and cellular requirements for muscle cell death in other animal models of muscular dystrophy.

While it has previously been proposed that α-dystrobrevin plays a structural role in the DGC [10–12], we provide the first direct evidence that α-dystrobrevin helps to biochemically stabilize the interaction of dystrophin with the dystroglycan complex. Prior immunohistochemical analyses in *adbn*$^{-/-}$ mice have suggested that all other DGC components are expressed at normal levels and localize properly to the sarcolemma [13]. Similarly, we found that total dystrophin levels were equivalent in control and *adbn*$^{-/-}$ skeletal muscle extracts, but reduced by 70% in DGC-enriched fractions from *adbn*$^{-/-}$ muscle. This result suggests that the association between dystrophin and the glycoprotein complex is compromised in the absence of α-dystrobrevin. Although the destabilization of the DGC may contribute to the muscle cell necrosis in *adbn*$^{-/-}$ mice, it appears that the degree of dystrophin destabilization is insufficient to render the membrane susceptible to damage, cause costamere disorganization or alter the functional performance of the skeletal muscle. Furthermore, the upregulation of the cytoskeletal protein syncoilin [38] may be providing compensatory structural stabilization to the sarcolemma in the absence of α-dystrobrevin.

In addition to the sarcolemma, α-dystrobrevin is also enriched at the neuromuscular junction (NMJ). Previous work has shown that *adbn*$^{-/-}$ mice exhibit defects in the maturation and maintenance of the postsynaptic membrane at the NMJ as the result of increased mobility and turnover of acetylcholine receptors (AChRs) [21,39]. Similarly, dystroglycan deficiency also disrupts the organization and stability of AChR clusters [40]. These studies suggest that the DGC is important for anchoring AChRs at synapses and maintaining postsynaptic receptor density at the NMJ. Our data illustrating

the instability of the DGC in *adbn*$^{-/-}$ mice provides a possible explanation for the increased AChR mobility. While acetylcholinesterase (AChE) mobility is also increased in *adbn*$^{-/-}$ mice [41], it is unclear whether this is an indirect result of changes in AChRs or whether α-dystrobrevin and the DGC play a direct role in AChE stability. Nonetheless, disruption of AChE stability could result in prolonged muscle hyperexcitability, which over time may contribute to the observed cell death in *adbn*$^{-/-}$ mice. In support of this idea, mutations in the *Caenorhabditis elegans* dystrobrevin-like gene cause hypercontractility, which leads to muscle degeneration when on a sensitized background [42].

Study of the *adbn*$^{-/-}$ mouse has provided insight into the pathological factors that contribute to the development of muscular dystrophy. The observation that muscle cell necrosis and functional deficits are separable phenotypes forces us to reconsider the traditional view that muscle cell death is a causative factor for muscle weakness in muscle diseases. Furthermore, the *adbn*$^{-/-}$ mouse suggests that membrane fragility is not the sole contributing factor for muscle cell death in DGC-related muscular dystrophies. Further studies are needed to compare the cellular and molecular differences between the *adbn*$^{-/-}$ mouse and other DGC-related mouse models in order to help dissect the mechanisms underlying the development of muscular dystrophies.

Acknowledgements

We thank Drs. J.R. Patel and Kurt Saupe for assistance with measurement of whole body tension and maximal exercise performance, respectively.

References

1. Ervasti JM (2007) Dystrophin, its interactions with other proteins, and implications for muscular dystrophy. Biochim Biophys Acta 1772: 108-117.

2. Petrof BJ, Shrager JB, Stedman HH, Kelly AM, Sweeney HL (1993) Dystrophin protects the sarcolemma from stresses developed during muscle contraction. Proc Natl Acad Sci U S A 90: 3710-3714.

3. Blake DJ, Weir A, Newey SE, Davies KE (2002) Function and genetics of dystrophin and dystrophin-related proteins in muscle. Physiol Rev 82: 291-329.

4. Durbeej M, Campbell KP (2002) Muscular dystrophies involving the dystrophin-glycoprotein complex: an overview of current mouse models. Curr Opin Genet Dev 12: 349-361.

5. Hack AA, Groh ME, McNally EM (2000) Sarcoglycans in muscular dystrophy. Microsc Res Tech 48: 167-180.

6. Barresi R, Campbell KP (2006) Dystroglycan: from biosynthesis to pathogenesis of human disease. J Cell Sci 119: 199-207.

7. Dwyer TM, Froehner SC (1995) Direct binding of Torpedo syntrophin to dystrophin and the 87 kDa dystrophin homologue. FEBS Lett 375: 91-94.

8. Ahn AH, Freener CA, Gussoni E, Yoshida M, Ozawa E, et al. (1996) The three human syntrophin genes are expressed in diverse tissues, have distinct chromosomal locations, and each bind to dystrophin and its relatives. J Biol Chem 271: 2724-2730.

9. Sadoulet-Puccio HM, Rajala M, Kunkel LM (1997) Dystrobrevin and dystrophin: an interaction through coiled-coil motifs. Proc Natl Acad Sci U S A 94: 12413-12418.

10. Yoshida M, Hama H, Ishikawa-Sakurai M, Imamura M, Mizuno Y, et al. (2000) Biochemical evidence for association of dystrobrevin with the sarcoglycan-sarcospan complex as a basis for understanding sarcoglycanopathy. Hum Mol Genet 9: 1033-1040.

11. Newey SE, Howman EV, Ponting CP, Benson MA, Nawrotzki R, et al. (2001) Syncoilin, a novel member of the intermediate filament superfamily that interacts with alpha-dystrobrevin in skeletal muscle. J Biol Chem 276: 6645-6655.

12. Mizuno Y, Thompson TG, Guyon JR, Lidov HG, Brosius M, et al. (2001) Desmuslin, an intermediate filament protein that interacts with alpha -dystrobrevin and desmin. Proc Natl Acad Sci U S A 98: 6156-6161.

13. Grady RM, Grange RW, Lau KS, Maimone MM, Nichol MC, et al. (1999) Role for alpha-dystrobrevin in the pathogenesis of dystrophin-dependent muscular dystrophies. Nat Cell Biol 1: 215-220.

14. Duclos F, Straub V, Moore SA, Venzke DP, Hrstka RF, et al. (1998) Progressive muscular dystrophy in alpha-sarcoglycan-deficient mice. J Cell Biol 142: 1461-1471.

15. Sasaoka T, Imamura M, Araishi K, Noguchi S, Mizuno Y, et al. (2003) Pathological analysis of muscle hypertrophy and degeneration in muscular dystrophy in gamma-sarcoglycan-deficient mice. Neuromuscul Disord 13: 193-206.

16. Durbeej M, Cohn RD, Hrstka RF, Moore SA, Allamand V, et al. (2000) Disruption of the beta-sarcoglycan gene reveals pathogenetic complexity of limb-girdle muscular dystrophy type 2E. Mol Cell 5: 141-151.

17. Araishi K, Sasaoka T, Imamura M, Noguchi S, Hama H, et al. (1999) Loss of the sarcoglycan complex and sarcospan leads to muscular dystrophy in beta-sarcoglycan-deficient mice. Hum Mol Genet 8: 1589-1598.

18. Pastoret C, Sebille A (1995) mdx mice show progressive weakness and muscle deterioration with age. J Neurol Sci 129: 97-105.

19. Cote PD, Moukhles H, Lindenbaum M, Carbonetto S (1999) Chimaeric mice deficient in dystroglycans develop muscular dystrophy and have disrupted myoneural synapses. Nat Genet 23: 338-342.

20. Hack AA, Lam MY, Cordier L, Shoturma DI, Ly CT, et al. (2000) Differential requirement for individual sarcoglycans and dystrophin in the assembly and function of the dystrophin-glycoprotein complex. J Cell Sci 113 (Pt 14): 2535-2544.

21. Grady RM, Zhou H, Cunningham JM, Henry MD, Campbell KP, et al. (2000) Maturation and maintenance of the neuromuscular synapse: genetic evidence for roles of the dystrophin--glycoprotein complex. Neuron 25: 279-293.

22. Ohlendieck K, Ervasti JM, Snook JB, Campbell KP (1991) Dystrophin-glycoprotein complex is highly enriched in isolated skeletal muscle sarcolemma. J Cell Biol 112: 135-148.

23. Williams MW, Bloch RJ (1999) Extensive but coordinated reorganization of the membrane skeleton in myofibers of dystrophic (mdx) mice. J Cell Biol 144: 1259-1270.

24. Reed P, Bloch RJ (2005) Postnatal changes in sarcolemmal organization in the mdx mouse. Neuromuscul Disord 15: 552-561.

25. Rybakova IN, Patel JR, Ervasti JM (2000) The dystrophin complex forms a mechanically strong link between the sarcolemma and costameric actin. J Cell Biol 150: 1209-1214.

26. Poon E, Howman EV, Newey SE, Davies KE (2002) Association of syncoilin and desmin: linking intermediate filament proteins to the dystrophin-associated protein complex. J Biol Chem 277: 3433-3439.

27. O'Neill A, Williams MW, Resneck WG, Milner DJ, Capetanaki Y, et al. (2002) Sarcolemmal organization in skeletal muscle lacking desmin: evidence for cytokeratins associated with the membrane skeleton at costameres. Mol Biol Cell 13: 2347-2359.

28. Brooks SV, Zerba E, Faulkner JA (1995) Injury to muscle fibres after single stretches of passive and maximally stimulated muscles in mice. J Physiol 488 (Pt 2): 459-469.

29. Carlson CG, Makiejus RV (1990) A noninvasive procedure to detect muscle weakness in the mdx mouse. Muscle Nerve 13: 480-484.

30. Gordon T, Stein RB (1988) Comparison of force and stiffness in normal and dystrophic mouse muscles. Muscle Nerve 11: 819-827.

31. Balaban B, Matthews DJ, Clayton GH, Carry T (2005) Corticosteroid treatment and functional improvement in Duchenne muscular dystrophy: long-term effect. Am J Phys Med Rehabil 84: 843-850.

32. Keeling RM, Golumbek PT, Streif EM, Connolly AM (2007) Weekly oral prednisolone improves survival and strength in male mdx mice. Muscle Nerve 35: 43-48.

33. Deconinck N, Dan B (2007) Pathophysiology of duchenne muscular dystrophy: current hypotheses. Pediatr Neurol 36: 1-7.

34. Warner LE, DelloRusso C, Crawford RW, Rybakova IN, Patel JR, et al. (2002) Expression of Dp260 in muscle tethers the actin cytoskeleton to the dystrophin-glycoprotein complex and partially prevents dystrophy. Hum Mol Genet 11: 1095-1105.

35. Thomas GD, Sander M, Lau KS, Huang PL, Stull JT, et al. (1998) Impaired metabolic modulation of alpha-adrenergic vasoconstriction in dystrophin-deficient skeletal muscle. Proc Natl Acad Sci U S A 95: 15090-15095.

36. Coral-Vazquez R, Cohn RD, Moore SA, Hill JA, Weiss RM, et al. (1999) Disruption of the sarcoglycan-sarcospan complex in vascular smooth muscle: a novel mechanism for cardiomyopathy and muscular dystrophy. Cell 98: 465-474.

37. Chao DS, Silvagno F, Bredt DS (1998) Muscular dystrophy in mdx mice despite lack of neuronal nitric oxide synthase. J Neurochem 71: 784-789.

38. McCullagh KJ, Edwards B, Poon E, Lovering RM, Paulin D, et al. (2007) Intermediate filament-like protein syncoilin in normal and myopathic striated muscle. Neuromuscul Disord

39. Akaaboune M, Grady RM, Turney S, Sanes JR, Lichtman JW (2002) Neurotransmitter receptor dynamics studied in vivo by reversible photo-unbinding of fluorescent ligands. Neuron 34: 865-876.

40. Jacobson C, Cote PD, Rossi SG, Rotundo RL, Carbonetto S (2001) The dystroglycan complex is necessary for stabilization of acetylcholine receptor clusters at neuromuscular junctions and formation of the synaptic basement membrane. J Cell Biol 152: 435-450.

41. Martinez P, Akaaboune M (2007) Acetylcholinesterase mobility and stability at the neuromuscular junction of living mice. Mol Biol Cell 18: 2904-2911.

42. Gieseler K, Mariol MC, Bessou C, Migaud M, Franks CJ, et al. (2001) Molecular, genetic and physiological characterisation of dystrobrevin-like (dyb-1) mutants of Caenorhabditis elegans. J Mol Biol 307: 107-117.

43. Sonnemann KJ, Fitzsimons DP, Patel JR, Liu Y, Schneider MF, et al. (2006) Cytoplasmic gamma-actin is not required for skeletal muscle development but its absence leads to a progressive myopathy. Dev Cell 11: 387-397.

44. Brooks SV, Faulkner JA (1988) Contractile properties of skeletal muscles from young, adult and aged mice. J Physiol 404: 71-82.